



Eidgenössische Technische Hochschule Zürich  
Swiss Federal Institute of Technology Zurich

A / S      Architecture  
                 and Building  
                 Systems

Jeremias Schmidli

# Numerical Energy Analysis of PV Modules as Adaptive Building Shading Systems

Master Thesis

ITA – Architecture and Building Systems  
Swiss Federal Institute of Technology (ETH) Zurich

Examiner: Prof. Dr. Arno Schlueter  
Supervisor: Prageeth Jayathissa

Zurich, May 30, 2016



# Acknowledgement

This master thesis represents the last building stone of my master's education at ETH Zurich. Therefore, I would like to sincerely thank everyone, who has supported me throughout my studies. First of all, I want to thank my supervisor Prageeth Jayathissa, who has been greatly supporting me during this thesis. I also want to express my gratitude to Prof. Dr. Arno Schlueter, for giving me the opportunity to write my thesis within the A/S Group. Next, I would like to thank Johannes Hofer, who was extremely helpful with radiation evaluations and photovoltaic simulations, as well as various general discussions on other simulations and their results. Furthermore, I want to acknowledge everyone in the A/S team, I had many interesting discussions and conversations with all of the group members. Finally, I would like to thank my family and friends, for supporting my at all times. Without them, I wouldn't have made it to where I am now.

# Abstract

Building integrated photovoltaic (BIPV), dynamic shading systems and adaptive envelopes are becoming increasingly important in modern building technology. The adaptive solar facade (ASF) project represents all three of them, as it is a dynamic shading system with integrated photovoltaic (PV) cells, forming an adaptive envelope. Thus, the ASF provides a promising technology for future energy efficient buildings.

This work presents a methodology to simultaneously calculate the building energy demand and the PV electricity production of a building with PV modules as adaptive building shading systems. A parametric model was built for dynamic evaluations and optimisations of such a system. A case study was then performed on a model representing the prototype of the ASF at the House of Natural Resources at ETH Zurich.

It was possible to find the optimising configurations of the described system as well as the corresponding building energy demand. Furthermore, various influences were evaluated including sensitivities on the building orientation, the geographic location, the control strategy, and the building system parameters. For the chosen base case evaluation, energy benefits of 9% were obtained when compared to a fixed solar facade at the most beneficial angle. The corresponding PV electricity output is able to compensate for 41% of the total building energy demand. The benefits are even larger for warmer regions than Zurich, as well as for buildings that have less efficient heating and cooling systems.

# Contents

List of Figures . . . . .	ix
List of Acronyms . . . . .	x
List of Symbols . . . . .	xi
<b>1 Introduction</b>	<b>1</b>
1.1 Motivation and Literature Review . . . . .	1
1.2 Problem Statement . . . . .	3
1.3 Objectives of Research . . . . .	3
1.4 Thesis Outline . . . . .	3
<b>2 Methodology</b>	<b>4</b>
2.1 Simulation Tool Selection . . . . .	4
2.1.1 Building Energy Simulation . . . . .	5
2.1.2 Radiation Simulation . . . . .	5
2.1.3 Photovoltaic Simulation . . . . .	6
2.2 Simulation Framework . . . . .	8
2.2.1 Combined Evaluation . . . . .	8
2.2.2 Parametric Simulation Model . . . . .	9
2.3 Case Study . . . . .	10
<b>3 Results and Discussion</b>	<b>13</b>
3.1 Base Case Evaluation . . . . .	13
3.2 Influence of Angle Actuation . . . . .	16
3.3 Comparison of Sun Tracking to Optimised Solution . . . . .	17
3.4 Sensitivity on Control Strategy Approach . . . . .	18
3.5 Orientation Analysis . . . . .	20
3.6 Location Analysis . . . . .	20
3.7 Sensitivity on Building System Parameters . . . . .	23
3.8 Evaluation of Different Combination Settings . . . . .	23
3.9 Potential of Independent Actuation . . . . .	25
<b>4 Conclusions</b>	<b>28</b>
<b>5 Outlook</b>	<b>31</b>

<b>A Usage of Simulation Environment</b>	<b>32</b>
A.1 Get ASF_Simulation Folder . . . . .	32
A.1.1 Git Set-Up . . . . .	32
A.2 Installation Guides . . . . .	33
A.2.1 Installing Rhino . . . . .	33
A.2.2 Installing Grasshopper . . . . .	33
A.2.3 Installing Python . . . . .	33
A.3 Grasshopper Simulations . . . . .	34
A.3.1 General Description of <i>main.gh</i> . . . . .	34
A.3.2 Set Geometry . . . . .	34
A.3.3 Geometry Calculations . . . . .	34
A.3.4 EnergyPlus Simulation . . . . .	35
A.3.5 Loop EnergyPlus . . . . .	36
A.3.6 Set Weather File . . . . .	36
A.3.7 Save Details of Weather File . . . . .	36
A.3.8 Loop LadyBug . . . . .	36
A.3.9 Set Evaluation Period . . . . .	36
A.3.10 Ladybug Solar Analysis . . . . .	37
A.3.11 Save Radiation Results . . . . .	37
A.4 Python Evaluation . . . . .	38
A.4.1 Main Python File . . . . .	38
A.4.2 Compare Results . . . . .	38
A.4.3 Post-Process Sun Tracking . . . . .	38
A.4.4 Create Further Visualisations . . . . .	38
A.4.5 Auxiliary Files . . . . .	38
A.5 First Time Set-Up of a Simulation . . . . .	39
A.6 Run Grasshopper Simulations . . . . .	39
A.6.1 General Simulation Set-Up . . . . .	40
A.6.2 Run a LadyBug Radiation Simulation . . . . .	40
A.6.3 Run an EnergyPlus Building Simulation . . . . .	41
A.7 Run Python . . . . .	41
<b>B Further Results</b>	<b>43</b>
B.1 Building Energy Analysis . . . . .	43
B.2 Further Visualisations of Radiation and PV results . . . . .	45
B.3 Tradeoffs Between Different Optimisation Strategies . . . . .	48
<b>Bibliography</b>	<b>52</b>

# List of Figures

1.1	Detailed overview of one ASF module [1] . . . . .	2
2.1	A simulation result showing module insolation from 12:00-13:00 on the 11th of August for a weather file of Kloten-Zurich and a specific module orientation. . . . .	6
2.2	Grid convergence evaluation, showing the deviations of the radiation in dependence of the grid size, time of the day and panel orientation. (a) shows the total radiation on the panels in dependence of the hour of the day, (b) depicts the same results, but normalized to the results with the smallest grid size, (c) presents the influence of the panel orientation, (d) plots the average deviation from the smallest grid size and (e) visualises all deviations with the usage of box-plots. . . . .	7
2.3	Work flow of the simulation framework . . . . .	9
2.4	Blackbox visualization of the parametric simulation model . .	10
2.5	Prototype of the adaptive solar facade on the house of natural resources . . . . .	12
3.1	Carpet plots detailing the optimal altitude angles to minimise the (a) heating demand, (b) cooling demand, (c) lighting demand, and (d) maximise PV electricity production. Figure (e) details the combinations for optimum building thermal management without PV production, (f) also includes the PV production. Small angles correspond to closed positions, whereas large angles represent open positions. The corresponding azimuth angles for each hour can be seen in the following Figure (3.2). . . . .	14

3.2	Carpet plots detailing the optimal azimuth angles to minimise the (a) heating demand, (b) cooling demand, (c) lighting demand, and (d) maximise PV electricity production. Figure (e) details the combinations for optimum building thermal management without PV production, (f) also includes the PV production. Negative angles correspond to the panels facing west, whereas positive angles represent east-facing panels. The corresponding altitude angles for each hour can be seen in the previous Figure (3.1). . . . .	14
3.3	Carpet plots detailing the net energy consumption. Each square represents the total energy consumption for that specific hour of the entire month. Red colours detail the energy demand, while blue colours detail the energy supply. . . . .	15
3.4	Energy benefits of the altitude actuation for the months of March (a), June (b) and September (c). Each plot displays one cumulative day in hourly resolution. The x-axis represents the altitude angles, the y-axis corresponds to the hour of the day, and the z-axis represents the energy benefit of the actuation, i.e. the difference in energy usage between the evaluated angle and the angle that yields the worst overall energy usage for each hour. . . . .	17
3.5	Comparison of optimised solution to sun-tracking. (a) Average radiation on panels compared to radiation without shading. While the radiation for sun-tracking is very similar to the radiation with the optimised angles, there are large losses caused by self-shading on the panels. (b) PV electricity production comparison. The optimised solution yields a significantly larger power output. (c) PV efficiency comparison. The optimised solution is able to stay at higher efficiencies than the sun-tracking approach. . . . .	18
3.6	Comparison of different control strategies. (a) Total energy demand per room area. (b) Energy difference to individually optimised solution. While the individually optimised solution is not physically feasible, it is well suited for comparison and to emphasize the tradeoffs between the different optimisations. . . . .	19
3.7	Energy demand in dependence of building orientation. (a) Total Energy Demand per room area, a south facing room has the lowest building energy demand while simultaneously maximising the PV-electricity production. (b) Energy Savings per room area of optimised solution compared to a fixed solar facade at 45° altitude. (c) Energy Savings per room area of optimised solution compared to a building without external shading. The energy benefit of the south-east facing ASF is the highest, mainly due to a better cooling performance. . . . .	21

3.8 Energy demand in dependence of building location. (a) Total Energy Demand per room area, Madrid yields the lowest building energy demand while simultaneously maximising the PV-electricity production. (b) Energy Savings per room area of optimised solution compared to a fixed solar facade at 45° altitude. (c) Energy Savings per room area of optimised solution compared to a building without external shading. The energy benefit of the ASF for the warm and sunny regions is much greater than for the colder regions, this is due to a higher significance of cooling and increased electricity production of the PV panels. . . . .	22
3.9 Sensitivity analysis of energy savings during one year. From left to right, sensitivities on heating COP, cooling COP, lighting load, and infiltration rate. The top row (a) shows the energy savings compared to a fixed solar facade at a 45° altitude angle, the bottom row (b) shows the energy savings compared to a room without shading or PV modules. The emphasized bar in every subplot corresponds to the basecase settings, all of them have the same height as they correspond to the same simulation. . . . .	24
3.10 Comparison of different combination settings. (a) shows the energy savings compared to a fixed facade at a 45° altitude, (b) shows the savings in comparison to a building with no external shading. . . . .	25
3.11 Cluster analysis of the ASF. The left column details the analysis with 2 clusters, whereas the right column corresponds to the 3 cluster analysis. (a) shows the average power use per room area for the month of June, (b) details the corresponding power difference, and (c) visualizes the total energy savings, averaged for the months of March, June, September and December. . . . .	27
B.1 Carpet plots detailing the optimal altitude angles to minimise the (a) heating demand, (b) cooling demand, (c) lighting demand, and (d) total building energy demand. Darker colours represent closed positions, whereas brighter colors correspond to open positions. To optimize heating and lighting, open positions are favorable, cooling is optimized by using closed positions. . . . .	44
B.2 Carpet plots detailing the optimal azimuth angles to minimise the (a) heating demand, (b) cooling demand, (c) lighting demand, and (d) total building energy demand. Cooling is minimized by blocking the sun, whereas lighting and heating are minimized by opening the facade to let the insolation in. . . . .	44

B.3 Carpet plots detailing the energy consumption during every hour of the year for the (a) heating demand, (b) cooling demand, (c) lighting demand, and (d) total building energy demand. . . . .	45
B.4 Angle visualisations, that optimise the altitude (top) and azimuth (bottom) angles for radiation (left) and PV electricity production (right). While the Radiation optimisation yields a symmetric pattern, the PV electricity optimisation deviates from the pattern that optimises the radiation in order to minimise longitudinal shading on the panels. . . . .	46
B.5 Comparison of PV electricity production with sun tracking to optimised solution. Top: Average power output for every month of the year. Bottom: Corresponding power difference. The difference is especially high during noon and in the afternoon. . . . .	46
B.6 Comparison of PV efficiency with sun tracking to optimised solution. Top: Average efficiency for every month of the year. Bottom: Corresponding efficiency difference. The difference is especially high during noon and in the afternoon. . . . .	47
B.7 Influence of optimisation strategy on heating demand. Top: Energy demand of heating in dependence of optimisation strategy. Bottom: Corresponding difference to heating optimisation. . . . .	48
B.8 Influence of optimisation strategy on cooling demand. Top: Energy demand of cooling in dependence of optimisation strategy. Bottom: Corresponding difference to cooling optimisation. . . . .	49
B.9 Influence of optimisation strategy on lighting demand. Top: Energy demand of lighting in dependence of optimisation strategy. Bottom: Corresponding difference to lighting optimisation. . . . .	49
B.10 Influence of optimisation strategy on PV electricity production. Top: Energy demand of PV electricity production in dependence of optimisation strategy (negative because production corresponds to a negative demand). Bottom: Corresponding difference to PV electricity optimisation. . . . .	50
B.11 Influence of optimisation strategy on building energy demand. Top: Building energy demand in dependence of optimisation strategy. Bottom: Corresponding difference to building energy demand optimisation. . . . .	50
B.12 Influence of optimisation strategy on net energy demand including PV electricity production. Top: Net energy demand in dependence of optimisation strategy. Bottom: Corresponding difference to overall optimisation. . . . .	51
B.13 Energy demand distribution at overall optimization. . . . .	51

# List of Acronyms

BIPV	Building Integrated Photovoltaics
PV	Photovoltaic
ASF	Adaptive Solar Facade
CIGS	Copper Indium Gallium Selenide
CAD	Computer-Aided Design
COP	Coefficient of Performance
HoNR	House of Natural Resources

# List of Symbols

$C$	Cooling Electricity Demand
$H$	Heating Electricity Demand
$L$	Lighting Electricity Demand
$PV$	Photovoltaic Electricity Production
$T_{cell}$	Temperature of Gridpoint on Panel
$T_{air}$	Ambient Air Temperature
$S$	Insolation
$HCL$	Total Heating, Cooling, and Lighting Electricity Demand
$E_{tot}$	Overall Electricity Demand ( $HCL - PV$ )

# Chapter 1

## Introduction

### 1.1 Motivation and Literature Review

Buildings are at the heart of society and currently account for 32% of global final energy consumption and 19% of energy-related greenhouse gas emissions [2]. Nevertheless, the building sector has a 50-90% emission reduction potential using existing technologies [2]. Within this strategy, building integrated photovoltaics (BIPV) have the potential of providing a substantial segment of a building's energy needs [3]. Even the photovoltaic (PV) industry has identified BIPV as one of the four key factors for the future success of PV [4].

Dynamic building envelopes have gained interest in recent years because they can save energy by controlling direct and indirect radiation into the building, while still responding to the desires of the user [5]. This mediation of solar insulation offers a reduction in heating / cooling loads and an improvement of daylight distribution [6]. Interestingly, the mechanics that actuate dynamic envelopes couples seamlessly with the mechanics required for facade integrated PV solar tracking. Further literature on dynamic building envelopes includes the work by Loonen et al. [7], where current building performance simulations of adaptive facades are reviewed and the lack of adaptability in building simulation tools is addressed. Single axis dynamic shading has been evaluated by Nielsen et al. [8], they are emphasizing the importance of numerical evaluations in facade design decisions.

Previous BIPV research analyses electricity production and building energy demand for static BIPV shading systems [9–16]. The performance of fixed PV shading devices in dependence of different angles was analysed for cooling and electrical performance with a simplified PV electricity model by Sun et al. [9]. That work was then extended to include different building orientations [10] . David et al. analysed the efficiency of fixed PV-shading devices, suggesting indices for comparison [11]. Fixed surrounding PV shad-

ing devices are found to be most efficient by Mandalaki et al. [12]. The same authors assess different PV simulation models and are able to show that extended electrical modelling is needed for complex PV geometry [13]. Furthermore, they also include visual comfort and find brise-soleil systems to perform best [14]. A first approach to assessing building energy demand with dynamic shading in combination with estimated PV electricity production is given by Jayathissa et al. [16].

The electricity production of PV shading devices has been evaluated for fixed angles by Freitas et al. [17]. They analysed different BIPV facade geometries and found horizontal louvers to perform best. An in-depth analysis of the electricity production of dynamic PV shading modules was evaluated for various design parameters with solar tracking by Hofer et al. [18].

This thesis expands on the previous work on dynamic PV shading modules [16, 18], by analysing dynamic PV shading systems and their influence on the building energy demand, while also taking into account mutual shading amongst modules and its effect on PV electricity generation. With this approach, it is possible to reduce efficiency degradation due to partial shading of PV modules [18].

The work presented in this thesis is applied in the context of the Adaptive Solar Facade (ASF) project [1]. The ASF is a lightweight PV shading system composed of copper indium gallium selenide (CIGS) panels, that can be easily installed on any surface of new or existing buildings. The panels can be individually actuated in both altitude and azimuth orientation. Figure 1.1 details the technology, showing the elements of one module. This thesis will present a methodology of simulating an ASF while simultaneously calculating the energy demand of the office space behind the facade.

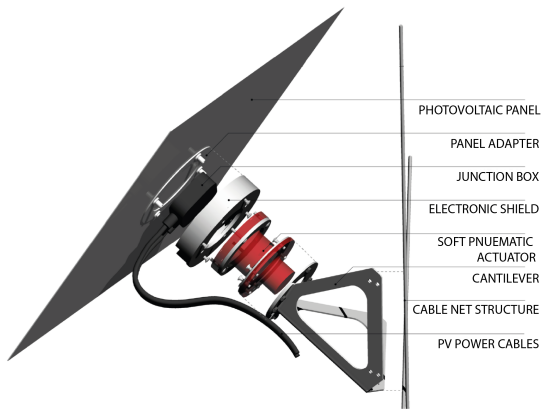


Figure 1.1: Detailed overview of one ASF module [1]

## 1.2 Problem Statement

Previous research has evaluated adaptive shading systems and building integrated photovoltaics. Combined evaluations, however, could not be found in existing literature. Even though there already are prototypes of the adaptive solar facade - with new ones to be built soon - a comprehensive way to numerically analyse the energy demand combined with the electricity production is missing. A parametric model to analyse PV modules as adaptive solar shading systems needs to be developed in order to optimise the control strategy of said prototypes. Optimum configurations are yet to be found and the corresponding energy benefits must be evaluated. Furthermore, the potential of PV modules as adaptive building shading systems needs to be quantized in more detail, in order to assess the hypothesis of the energy benefits from the general concept. Finally, different parameters must be evaluated to assess the effects of building orientation, possibilities and limits of current simulation tools, as well as various control strategy approaches.

## 1.3 Objectives of Research

Based on the problem statement, the objectives are to

- Develop a modelling framework to simulate the energetic performance of adaptive photovoltaic envelopes
- Find the best configurations to minimise the net building energy demand
- Assess effects of the building orientation, system parameters, location, and simulation strategies
- Suggest factors that must be taken into account to find the optimum control strategy

## 1.4 Thesis Outline

Chapter 2 introduces the methodology used within this thesis and describes the approaches taken for the building simulations, radiation and PV analysis, as well as the combination of the two separate simulations. In Chapter 3, the results of the building simulation and the electricity production are presented and different influences are shown and discussed. The work is summarized and concludes in Chapter 4 and an outlook for further research is given in Chapter 5.

## Chapter 2

# Methodology

This chapter describes the methodology used to find the optimum configurations of the ASF. In general terms, the optimum configuration must correspond to the following optimisation problem that has to be solved for PV modules as adaptive building shading systems:

$$\text{minimise}(C + H + L - PV) \quad (2.1)$$

Where  $C$  is the electricity needed for cooling,  $H$  is the electricity used for heating,  $L$  is the lighting power demand and  $PV$  represents the electricity production.

An evaluation of the tools that were selected and how they are combined to create a modelling framework is given and details of the simulation methodology are described.

### 2.1 Simulation Tool Selection

To study the electricity generation and building energy consumption, a 3D geometry of the room and the solar facade is built using the Rhinoceros software [19], and its parametric modelling plugin Grasshopper [20]. Rhinoceros is a state of the art computer-aided design (CAD) software, which can be used to generate complex geometries, such as the ASF. Grasshopper, on the other hand, provides a visual programming language with a wide range of add-ons, detailed in Sections 2.1.1 and 2.1.2. It is therefore particularly suited for simulations that are evaluating geometric structures. The simulation can then be split up into three parts, namely *building energy simulations*, *radiation simulations* and *photovoltaic simulations*, which will be described in the following subsections. While Grasshopper is well suited for running simulations, it is not very suited for post-processing the data. The post-processing and optimisation were therefore done in Python, a programming language with powerful scientific packages, a simple syntax, extended documentation, and a very active community.

### 2.1.1 Building Energy Simulation

There are various building energy analysis engines, such as EnergyPlus [21] or TRNSYS [22]. As EnergyPlus is open source, widely used, and well documented, it was chosen as the building simulation engine for all simulations within this thesis. There are multiple ways of connecting Grasshopper to EnergyPlus. Within this work, mainly DIVA [23] and Honeybee [24] were evaluated. While Honeybee provides a large range of settings and adaptability, its computational speed is significantly slower than DIVA. Therefore, and for its simplicity, DIVA was chosen to connect Grasshopper with EnergyPlus. In EnergyPlus, the geometric solar facade is interpreted as an external shading system. Simulations are performed for a whole year at fixed angle positions, outputting hourly values of energy use for heating, cooling and lighting. Optimum positions can then be found by comparing the electricity demand during every hour for all combinations.

### 2.1.2 Radiation Simulation

A solar radiance simulation is run using Ladybug [24], which is another Grasshopper plugin. It includes various components to process weather data and calculate radiation on surfaces based on an automatically generated or a predefined mesh. Ladybug uses Radiance [25] to determine the incident insolation on the solar facade. This approach enables the calculation of solar irradiance on the modules with high spatial resolution including the effect of module mutual shading as seen in Figure 2.1. The radiation is analysed for cumulative monthly hours for the whole year.

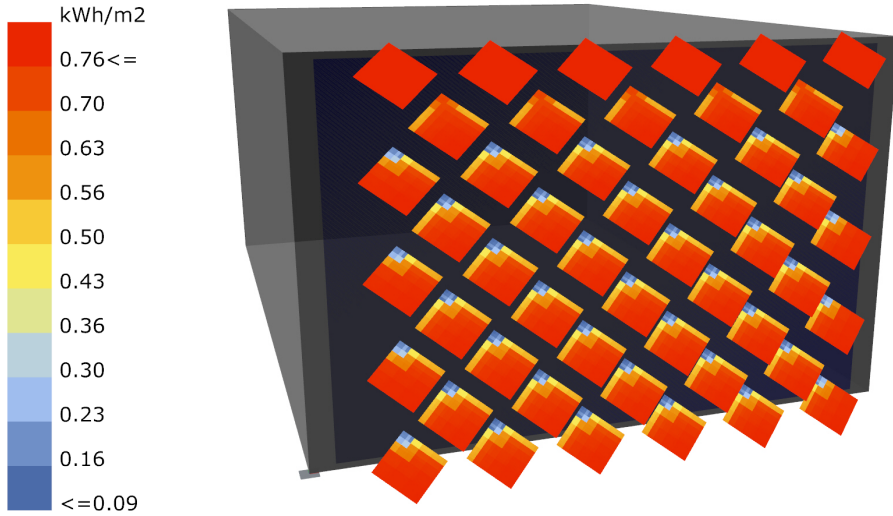


Figure 2.1: A simulation result showing module insolation from 12:00-13:00 on the 11th of August for a weather file of Kloten-Zurich and a specific module orientation.

### Grid Convergence

A grid convergence study was conducted to determine the effect of the grid size on the accuracy of the radiation results. Generally, larger grid sizes yield faster computational speeds, at the cost of lower accuracy. Figure 2.2 shows the grid size dependency of the total radiation on the ASF. The colours in the first two plots on the upper left ((a) and (b)) represent the hours of the day. One can see in the second plot (b), where the radiation is normalized to the results when the grid size is 12.5 mm, that the simulations are significantly more accurate for morning and evening hours. This is caused by increased self-shading at midday hours. The colours in the third plot on the left (c) show the dependency on different combinations. No clear pattern could be found here. Finally, the average deviation is depicted in the fourth plot on the left (d) and a box-plot with all deviations is shown on the right (e). It can be seen that a smaller grid size leads to larger deviations. While for a grid size of 400 mm the average deviation is over 10%, the deviation goes down to below 1% for a grid size of 25 mm. 25 mm was therefore taken as the grid size of all simulations, as it gives accurate results, while still being computationally feasible.

#### 2.1.3 Photovoltaic Simulation

The electrical model of the PV cells builds upon the methodology presented in [18], which is using the standard equivalent circuit model to calculate sub-

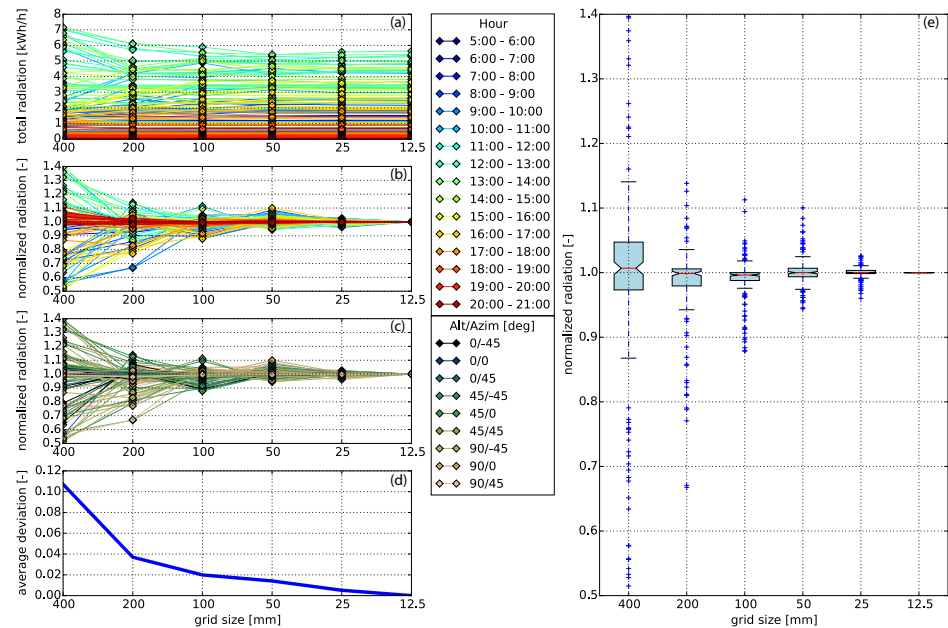


Figure 2.2: Grid convergence evaluation, showing the deviations of the radiation in dependence of the grid size, time of the day and panel orientation. (a) shows the total radiation on the panels in dependence of the hour of the day, (b) depicts the same results, but normalized to the results with the smallest grid size, (c) presents the influence of the panel orientation, (d) plots the average deviation from the smallest grid size and (e) visualises all deviations with the usage of box-plots.

cell I-V curves with a single diode, one series, and one shunt resistance [26]. For the work in [18], the PV simulation was implemented in MATLAB. For the work in this thesis, the MATLAB code was adjusted to match the new radiation simulations and then translated to python, in which the rest of the framework is written (details in Section 2.2). PV electricity production is calculated based on a reference module. In addition to the irradiation dependency, the PV simulation includes temperature dependency. The temperature is estimated as suggested in [27] with the following equation:

$$T_{cell} = T_{air} + \left( \frac{T_{cell}^0 - T_{air}^0}{S^0} \right) S_{cell} \quad (2.2)$$

where  $T_{cell}$  is the temperature of each grid point on the module,  $T_{air}$  is the ambient temperature,  $T_{cell}^0$  is the temperature of the cell at reference insolation  $S^0 = 800 \frac{W}{m^2}$  and reference air temperature  $T_{air}^0 = 20^\circ C$ , and  $S_{cell}$  is the insolation of each gridpoint in  $\frac{W}{m^2}$ . The value of  $T_{cell}^0$  was estimated using thermal images of the solar facade and typical values given in [27] to be  $38^\circ C$ .

## 2.2 Simulation Framework

In order to combine the single simulations, an evaluation framework was built with the use of Grasshopper and Python. In the following, details on how the combination was done and on the resulting parametric simulation model are given. A detailed description of the simulation framework usage can be found in Appendix A.

### 2.2.1 Combined Evaluation

While the building energy and the radiation simulations are conducted within Grasshopper, the PV calculations take place within Python. In pursuance of a simple combination of these individual simulations, a framework is necessary that follows the corresponding workflow shown in Figure 2.3. For this end, a folder structure was created to manage the files that are written both in Grasshopper and Python. There are two main files for the combined evaluation, one Grasshopper, and one Python file. In the Grasshopper file, all the parameters can be set and the simulations can be started. After the building energy and the radiation simulations are finished, the corresponding results are read by Python, where the PV electricity production is calculated and the results are combined. The combination of the building energy analysis with the PV electricity results is done by cumulatively combining the building energy results to correspond to the PV analysis format. With this, the net energy usage of the room including the PV electricity production of the ASF can be given for monthly hours as described in equation 2.1.

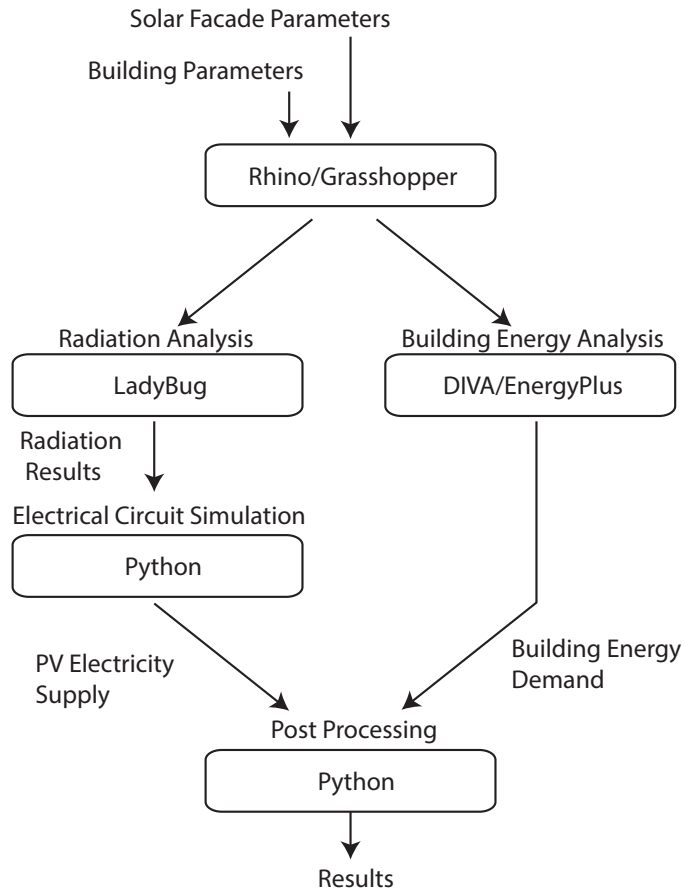


Figure 2.3: Work flow of the simulation framework

### 2.2.2 Parametric Simulation Model

Because of the many influences on simulations, the evaluation environment was built as a parametric simulation model. The parameters that can be set and the outputs of the simulation model are shown in Figure 2.4. The geographical location of the simulation is given by an epw weather file, out of which all relevant information is automatically extracted. The building system can be varied according to the DIVA parameter inputs, that is heating and cooling coefficient of performance (COP), infiltration rate, lighting power, fresh air, material type and occupancy. The direction which the building and the facade are facing can be set with a single number representing the deviation from south. Geometry settings are available for the ASF as well as for the building, enabling to easily evaluate every room size and facade layout. The actuation range is set by defining the azimuth and altitude angles, that will be evaluated. An additional input provides the

possibility to split up the facade into multiple panel clusters, thus providing the possibility to account for the independent actuation of the panels. Finally, the radiation grid size can be set, which influences accuracy of the radiation results and computational speed at the same time, as described in Section 2.1.2.

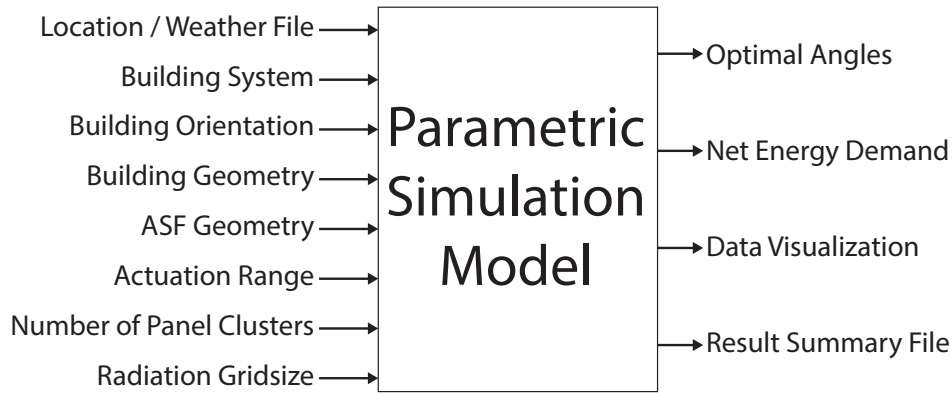


Figure 2.4: Blackbox visualization of the parametric simulation model

## 2.3 Case Study

A case study was conducted for a room and facade representing the prototype of the ASF at the house of natural resources (HoNR) [1]. The solar facade consists of 400 mm CIGS square panels that can rotate in two degrees of freedom. On the horizontal axis, the panels can move from 0° (closed) to 90° (open), whereas on the vertical axis, they can move from -45° to 45°.

Simulations are run for different angle combinations, with a weather file for Kloten-Zurich, Switzerland. There are two base-cases for the simulations. The first one consists of 49 different angle combinations (i.e. seven azimuth and seven altitude angles, with a step size of 15°), which is used for detailed evaluations of the angle positions. The second base-case consists of 25 angle combinations (five azimuth and five altitude angles), this case is used for the comparison of different system parameters. Simulations are done for average days of every month of the year with a south facing facade, and the results are then compared to control strategies where the angles are fixed or follow sun tracking. Furthermore, the sensitivity of various parameters, such as building orientation, geographical location, and COP of the heating/cooling system is evaluated.

A summary of the parameters that were used for the simulations is shown in Table 2.3, all walls other than the front wall were approximated as adi-

abatic. A picture of the ASF prototype installed at the HoNR can be seen in Figure 2.5.

Parameter	Value	Unit
<b>Building Dimensions</b>		
Width	4.9	m
Depth	7	m
Height	3.1	m
Horizontal Glazing	91.83	%
Vertical Glazing	96.77	%
<b>Building System</b>		
Heating COP	4	—
Cooling COP	3	—
Lighting Load	11.74	W/m <sup>2</sup>
Infiltration Rate [28]	1	1/h
Fresh Air [28]	0.016	m <sup>3</sup> /s per person
People	0.1	1/m <sup>2</sup>
Equipment	4	W/m <sup>2</sup>
Heating Setpoint	22	°C
Cooling Setpoint	26	°C
Lighting Control	300	lux
R-Value of Exterior Wall <sup>1</sup>	3.61	K · m <sup>2</sup> /W
R-Value of Window <sup>2</sup>	0.585	K · m <sup>2</sup> /W
Solar Heat Gain Coefficient of Window <sup>2</sup>	0.691	—
Visible Light Transmittance of Window <sup>2</sup>	0.744	—
<b>Facade Dimensions</b>		
Panel Size	400	mm
Panel Spacing	500	mm
Panel Offset	400	mm
Number of Panels	50	—
<b>Facade Simulation</b>		
Solar Reflectance <sup>3</sup>	0.5	—
Visible Reflectance <sup>3</sup>	0.5	—
Grid Size	25	mm
Distance from Base <sup>4</sup>	0.5	mm

Table 2.1: Parameters used for Simulations

<sup>1</sup>Corresponds to: *ASHRAE\_90.1-2007\_Climate\_Zone\_4-8\_Exterior\_Wall\_R-13 + R-7.5*

<sup>2</sup>Corresponds to: *Dbl LoE (e2=.2) Clr 3mm/13mm Arg*

<sup>3</sup>Only the EnergyPlus analysis with DIVA is able to include reflectance. Ladybug does not take reflectance into account.

<sup>4</sup>This value represents the distance from the panels used for the radiation calculations.



Figure 2.5: Prototype of the adaptive solar facade on the house of natural resources

# Chapter 3

## Results and Discussion

With the fully functional parametric model, various aspects of dynamic PV shading systems were evaluated for the ASF case study. This chapter presents and discusses the results of these evaluations. First, the base case is evaluated, visualizing the optimisation and the main outputs of the parametric model. Next, the influence of the angle actuation is discussed and the optimisation for PV electricity output is compared to an approach using sun-tracking. This is followed by sensitivity evaluations on the building orientation, the building location, and various building system parameters. Finally, the influence of different combination settings is shown and the potential of independent actuation is evaluated.

### 3.1 Base Case Evaluation

By combining results for building energy simulations and PV electricity production, the overall optimum configurations can be found. Figures 3.1 and 3.2 detail carpet-plots of the facade optimised to maximise PV generation, and minimise heating, cooling and lighting demands independently. The simulation was done for a base case with a total of 49 angle combinations with seven different states for the altitude and the azimuth angles, i.e. a step size of  $15^\circ$ . For simplicity, the altitude angles are presented separately to the azimuth angles in Figure 3.1 and Figure 3.2, respectively.

In the altitude angle visualization it can be seen how open configurations (light coloured) are chosen to minimise the building heating (Fig. 3.1a) and lighting (Fig. 3.1c) demand. Likewise, closed configurations (dark colours) are the preferred solutions to minimise the cooling demand (Fig. 3.1b). The PV optimisation tends to choose more open angles, corresponding to the minimisation of longitudinal shading as will be described in Section 3.3. In Figure 3.1e, the angles that optimise the overall building demand are shown. The optimisation chooses open positions at hours where heating and lighting are important, whereas closed positions are used for hours where cooling is

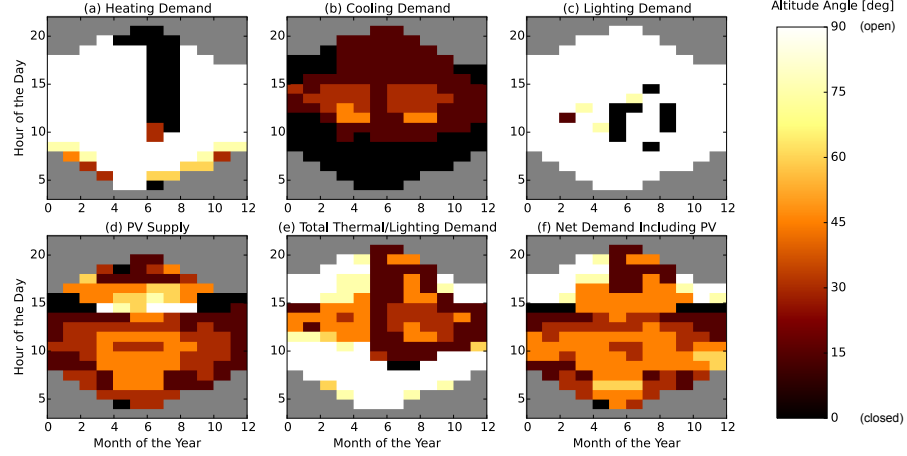


Figure 3.1: Carpet plots detailing the optimal altitude angles to minimise the (a) heating demand, (b) cooling demand, (c) lighting demand, and (d) maximise PV electricity production. Figure (e) details the combinations for optimum building thermal management without PV production, (f) also includes the PV production. Small angles correspond to closed positions, whereas large angles represent open positions. The corresponding azimuth angles for each hour can be seen in the following Figure (3.2).

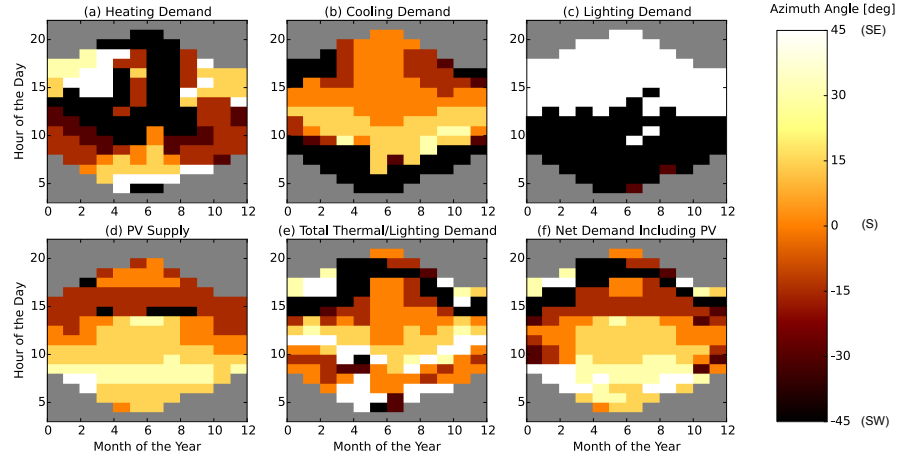


Figure 3.2: Carpet plots detailing the optimal azimuth angles to minimise the (a) heating demand, (b) cooling demand, (c) lighting demand, and (d) maximise PV electricity production. Figure (e) details the combinations for optimum building thermal management without PV production, (f) also includes the PV production. Negative angles correspond to the panels facing west, whereas positive angles represent east-facing panels. The corresponding altitude angles for each hour can be seen in the previous Figure (3.1).

dominant. The configurations for total energy minimisation - including the PV electricity production - are depicted in Figure 3.1f. It can be seen that there is a conflict in the summer evenings between minimising lighting and cooling demands. Likewise, there is a conflict between heating and PV production during the winter months. The overall energy optimisation shows a strong tendency to follow the optimal PV production pattern. This, however, changes if the building system becomes more inefficient. Less efficient heating, for example, would result in configurations optimised for heating overpowering those of PV electricity generation.

Similar patterns can be seen for the azimuth variations (Fig. 3.2). The azimuth angles correspond to the deviation from the building facade normal. As described in Section 2.3, the simulation was done for a south-facing facade. This means an angle with a positive sign represents the panels facing towards south-east (bright colours), whereas negative angles represent the panels facing towards south-west (dark colours). It can be seen that for heating and lighting, the facade takes positions that let the sun in, whereas for cooling the facade follows a sun-tracking pattern which prevents radiation from entering the room. The PV optimisation also follows a sun-tracking pattern, though with a deviation towards facing east. This is caused by the PV-layout and the effects of longitudinal shading [18]. The optimisation minimises longitudinal shading in order to maximise PV electricity production.

Figure 3.3 shows the net energy use at these optimum angles. (a) shows that heating is mainly dominant in the winter and in the mornings, cooling

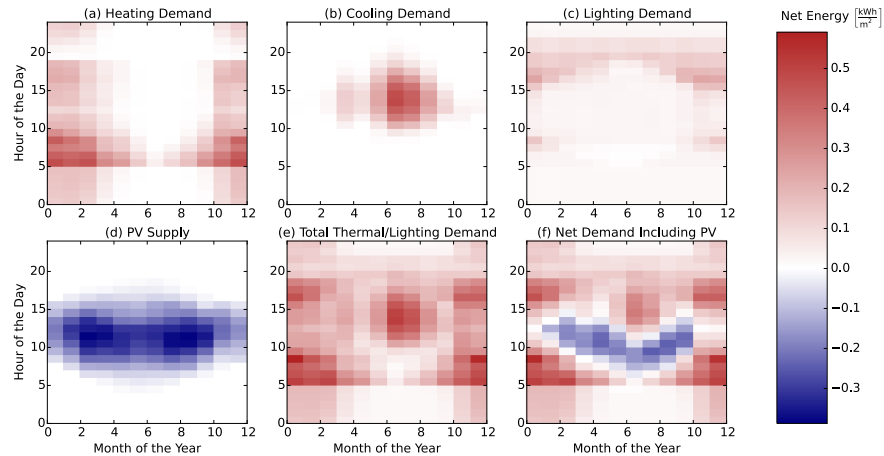


Figure 3.3: Carpet plots detailing the net energy consumption. Each square represents the total energy consumption for that specific hour of the entire month. Red colours detail the energy demand, while blue colours detail the energy supply.

(b) is primarily needed in the summer afternoons, lighting (c) at hours of low or no solar insolation, whereas PV electricity production (d) is dominant at hours with high solar insolation. (e) shows the total building energy demand and (f) visualizes the net energy demand including the PV electricity production. It can be seen that there is a net negative energy demand for most sunlit hours, meaning that the ASF is generating more energy than is used by the building for these hours.

Overall, the optimization yields an energy benefit of 9% compared to the best performing fixed solar facade solution, and the PV electricity production is able to compensate for 41% of the total building energy demand. Further visualisations of the building energy demand and the corresponding optimum positions can be found in Appendix B.1.

## 3.2 Influence of Angle Actuation

In order to analyse the influence of the actuation, three-dimensional plots can be used to display all evaluated configurations and their corresponding energy benefit. In Figure 3.4, the energy benefits of the altitude actuation are visualized for the months of March (a), June (b) and September (c). Each plot displays one cumulative day in hourly resolution. The x-axis represents the altitude angles (19 different angles were evaluated with a step size of  $5^\circ$ ), the y-axis corresponds to the hour of the day, and the z-axis represents the energy benefit of the actuation, i.e. the difference in energy usage between the evaluated angle and the angle that yields the worst overall energy usage for each hour. It can be seen that the energy benefit is by far the largest around noon. Furthermore, positions that are rather closed tend to have the highest influence for the said mid-day hours. Open positions normally yield the worst benefits, except for some early morning or evening hours, where heating and lighting become important.

This overall behaviour corresponds well to the previously described results, that are depicted in Figure 3.1, and shows why the angles that yield the optimum total energy, generally match the angles that optimise cooling and PV electricity production. A further interesting observation that can be made from this figure is the discontinuous curves for midday hours in summer. At an altitude angle of around  $30^\circ$ , the energy benefit reduces over-proportionally. This is caused by the PV electricity production, larger angles will increase longitudinal shading and therefore over proportionally reduce the energy yield.

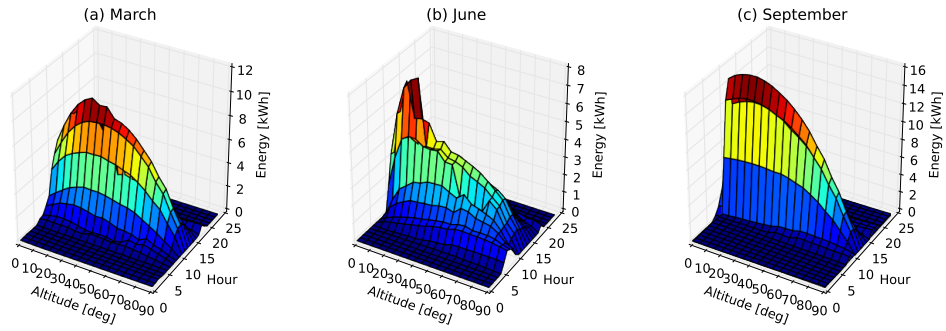


Figure 3.4: Energy benefits of the altitude actuation for the months of March (a), June (b) and September (c). Each plot displays one cumulative day in hourly resolution. The x-axis represents the altitude angles, the y-axis corresponds to the hour of the day, and the z-axis represents the energy benefit of the actuation, i.e. the difference in energy usage between the evaluated angle and the angle that yields the worst overall energy usage for each hour.

### 3.3 Comparison of Sun Tracking to Optimised Solution

As described in Section 3.1, the optimisation of the PV electricity production were different from angles that would correspond to sun-tracking. To evaluate this difference, simulations using sun-tracking were compared to the optimising simulations, that are evaluating 49 different combinations (i.e. 7 different azimuth and altitude angles).

Figure 3.5a shows the radiation on the panels and compares it to the radiation that would be incident if there were no self-shading. It can be seen that while the radiation with sun-tracking is similar to the optimised solution, there are large losses in summer due to the self-shading. The total radiation on the panels is lower in summer than in spring and autumn. This can be explained by the higher altitude of the sun during summer months. The higher sun position results in increasing self-shading.

Figure 3.5b shows the PV electricity production for the two different control strategies, whereas the corresponding efficiencies are compared in Figure 3.5c. The PV electricity production - as well as the corresponding efficiency - of the optimised solution is significantly higher than the sun-tracking solution in the afternoon hours. This is caused by the layout of the PV panels, longitudinal shading causes high power losses [18], thus the optimised solution decreases the longitudinal shading compared to sun-tracking. Therefore, an optimising solution should be preferred over a sun-tracking approach for control strategy considerations. Finally, the temperature de-

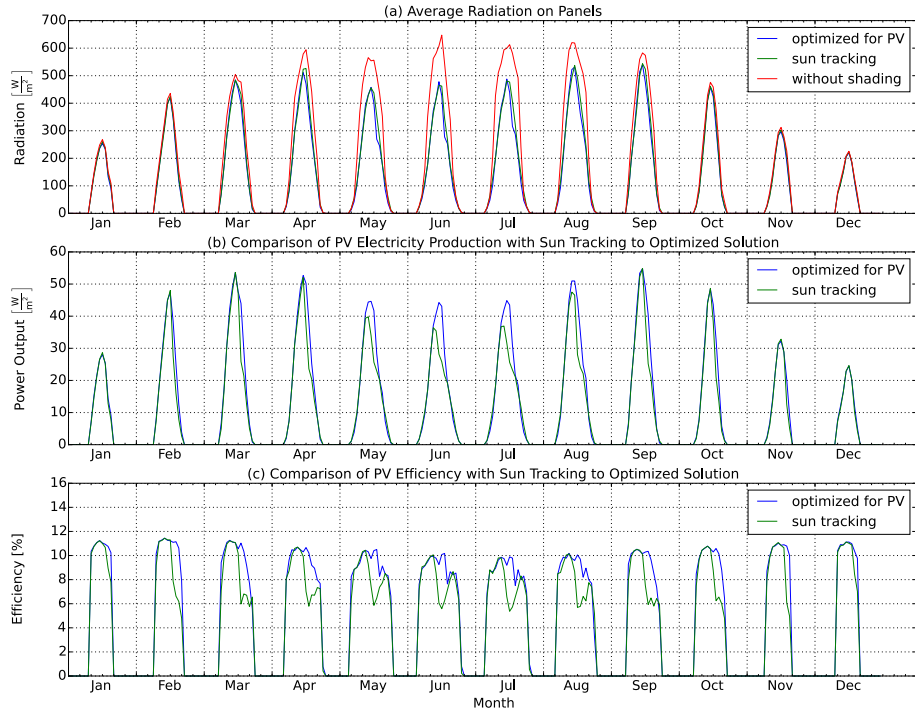


Figure 3.5: Comparison of optimised solution to sun-tracking. (a) Average radiation on panels compared to radiation without shading. While the radiation for sun-tracking is very similar to the radiation with the optimised angles, there are large losses caused by self-shading on the panels. (b) PV electricity production comparison. The optimised solution yields a significantly larger power output. (c) PV efficiency comparison. The optimised solution is able to stay at higher efficiencies than the sun-tracking approach.

pendency of the PV electricity model can be observed from the graph that is detailing the efficiency, even though the radiation in the winter months is significantly lower than during the rest of the year, the corresponding efficiency is comparatively high because of the lower temperatures in the winter months.

### 3.4 Sensitivity on Control Strategy Approach

To evaluate further possibilities and limitations of the control strategy of the ASF, the tradeoffs between different strategies were visualised. Figure 3.6a shows the total energy demand used for heating, cooling, and lighting, the PV electricity production, as well as the total building demand and the net energy demand (building demand minus PV electricity production)

for various control strategies. In Figure 3.6b the corresponding differences in energy of every control strategy to the individually optimised solution is shown. Even though the individual optimisation is not physically feasible, it is included in the evaluation because it serves as a good reference case, and tradeoffs between the different optimisation strategies can nicely be visualized. As expected, the overall optimisation has the smallest deviations from the individually optimised results. When comparing the different control strategies, one can see that especially cooling and PV need to be optimised, while the heating and lighting demand have a lower sensitivity on the control strategy. Another observation that can be gained is that the optimisation for cooling is not very beneficial for the PV electricity production. This corresponds to the results in the previous Section (3.3) and is caused by the longitudinal shading, which the cooling optimisation does not take into account. However, the optimisation for PV electricity production has a smaller negative influence on the cooling demand.

This graph is part of the parametric simulation model, and can easily be adjusted to evaluate different building system parameters, as well as time periods. Further figures that visualise the same behaviour can be found in Appendix B.3.

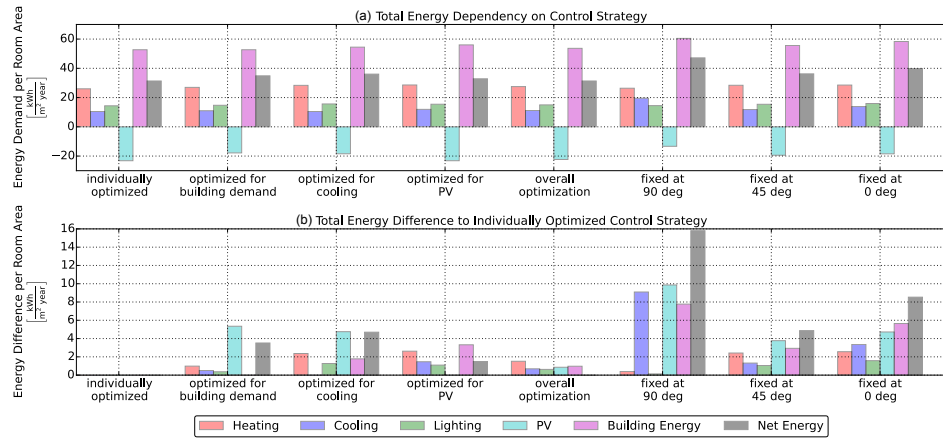


Figure 3.6: Comparison of different control strategies. (a) Total energy demand per room area. (b) Energy difference to individually optimised solution. While the individually optimised solution is not physically feasible, it is well suited for comparison and to emphasize the tradeoffs between the different optimisations.

### 3.5 Orientation Analysis

Evaluations of the facade for different building orientations were done with the base case of 5 azimuth and 5 altitude angles, corresponding to a total of 25 different combinations. This case was chosen in order to increase computational speed. In comparison to the optimisations with 49 combinations, simulations take less than half the time.

Figure 3.7 shows the performance of the building and the facade for west, south-west, south, south-east and east orientations. (a) details the total energy demand for the optimised solution, as expected, the south facing facade produces the most electricity. It also has the lowest building energy consumption, mainly because of a low energy demand for heating and cooling. It was found that the PV apertures should be oriented parallel to the upper left edge for facades that are west or south-west oriented, whereas they should be oriented parallel to the upper right edge for east or south-east oriented facades. This is caused by the shading patterns. Longitudinal shading needs to be prevented as described in Section 3.3. Furthermore, it can be observed that an east facing building uses less heating than a west facing building, which could be explained by the previous observation that heating is most important during morning hours. For similar reasoning, the east facing building needs more cooling energy than the west facing building because the room heats up in the morning and will not naturally cool down before the outdoor temperatures decrease in the evening. Interestingly, PV production is higher for the west facing facade than for the east facing facade. The cause for this is probably because of conflicts in optimising cooling and PV electricity production at the same time, as cooling is more dominant for the east facing building.

As for the ASF performance, the south-east facing facade yields the highest energy benefits. This becomes apparent when comparing the energy savings of the ASF to a fixed facade at a  $45^\circ$  altitude angle, or to a building with no external shading, as described in Figure 3.7 (b) and (c), respectively. It can clearly be seen, that this performance increase mainly comes from the high cooling demand. The benefits of the facade for the cooling energy use outweigh the lower benefit of the PV electricity supply.

### 3.6 Location Analysis

Similarly to the orientation analysis, the location of the building was evaluated. In Figure 3.8, the corresponding energy performance of an ASF is shown for the locations Helsinki, Zurich, Madrid, and Cairo. (a) shows the net energy demand for the different locations, it can clearly be seen that the further south a building is, the higher the cooling load and the lower the heating demand. The lighting however is similar in all cases. Interestingly,

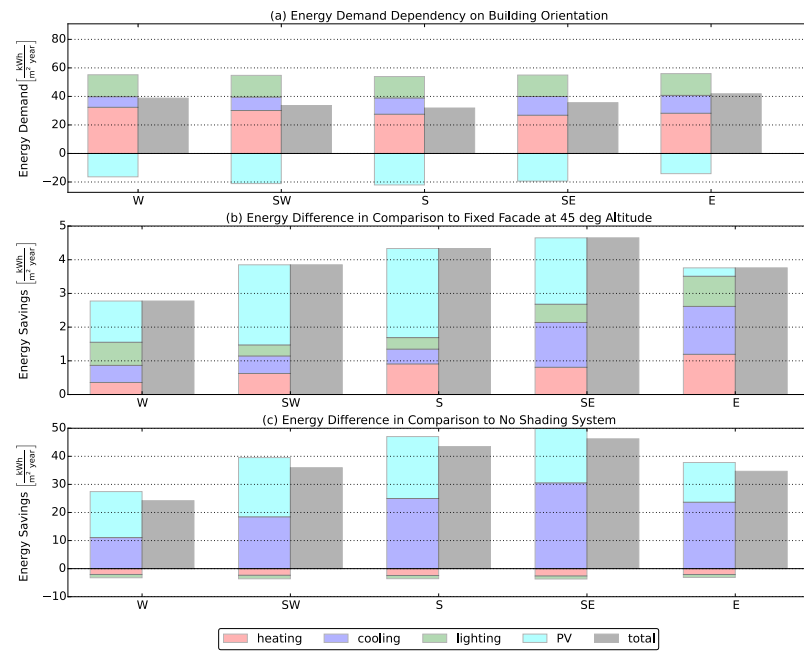


Figure 3.7: Energy demand in dependence of building orientation. (a) Total Energy Demand per room area, a south facing room has the lowest building energy demand while simultaneously maximising the PV-electricity production. (b) Energy Savings per room area of optimised solution compared to a fixed solar facade at 45° altitude. (c) Energy Savings per room area of optimised solution compared to a building without external shading. The energy benefit of the south-east facing ASF is the highest, mainly due to a better cooling performance.

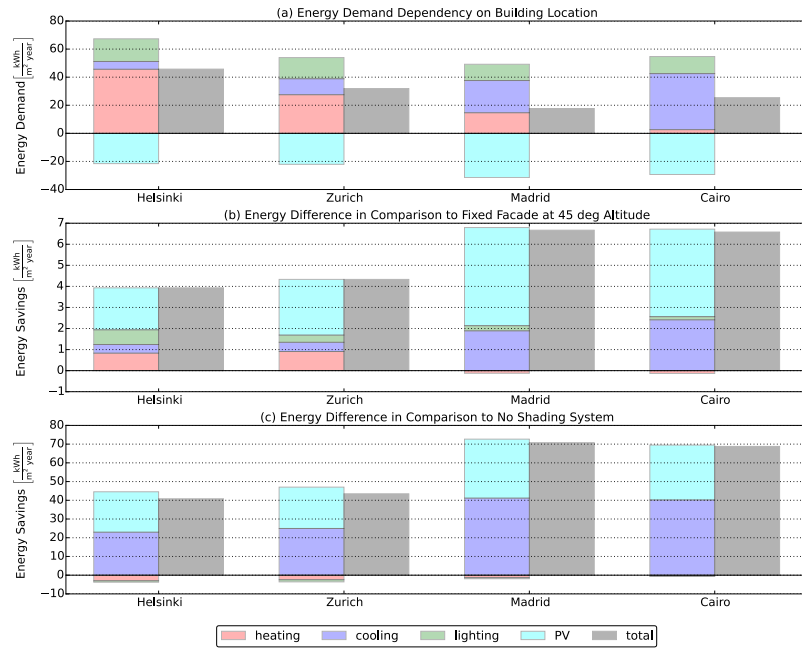


Figure 3.8: Energy demand in dependence of building location. (a) Total Energy Demand per room area, Madrid yields the lowest building energy demand while simultaneously maximizing the PV-electricity production. (b) Energy Savings per room area of optimised solution compared to a fixed solar facade at 45° altitude. (c) Energy Savings per room area of optimised solution compared to a building without external shading. The energy benefit of the ASF for the warm and sunny regions is much greater than for the colder regions, this is due to a higher significance of cooling and increased electricity production of the PV panels.

the PV electricity output is highest in Madrid. This can be explained by the altitude of the sun, in Cairo the average altitude is higher and therefore also the self-shading on the panels. As Madrid also shows the lowest net building energy demand, it can be said that the system is most efficient for this location. An analysis of the energy savings visualizes the impact of the location on the performance of the ASF even better. Therefore, the energy savings compared to a fixed solar facade at a 45° altitude angle and to a building without external shading are shown in Figure 3.8 (b) and (c), respectively. The warm and sunny locations of Madrid and Cairo have significantly larger energy savings than the ones in Helsinki and Zurich. This is caused by the large benefits of the ASF on reducing cooling as well as increasing the PV electricity output.

### 3.7 Sensitivity on Building System Parameters

A sensitivity analysis was done for the heating coefficient of performance (COP), cooling COP, lighting load, and infiltration rate. The results are shown in Figure 3.9. Figure 3.9a shows the energy savings per square meter of room area compared to a fixed solar facade at an angle of  $45^\circ$ , whereas Figure 3.9b shows the energy savings compared to a building without any PV modules or shading devices. The highlighted bar in each subplot represents the base case of the simulation with the same settings, therefore it has the same height for each parameter evaluation in the same row and serves as a reference. It can be seen that while the heating and cooling COP have large influences on the energy savings, the influence of the lighting load and the infiltration rate are significantly smaller. Especially a low COP for heating and cooling have a strong impact on the performance. For cooling, it becomes clear that an ASF is especially beneficial with inefficient cooling. As for the heating, it depends on the comparison case. While the energy savings are larger for a small heating COP when comparing it to a fixed solar facade at a  $45^\circ$  angle, they are smaller when comparing it to a building without external shading. This can be explained with the importance of heating for each of the two reference cases. A building without any shading naturally has a lower heating demand than a building with shading. When the heating COP is very small, which means that the energy demand for the heating is larger, it is relatively more efficient to have a building without shading than with shading. However, an ASF is still beneficial, as even with the lowest evaluated heating COP of 1 - corresponding to electrical heating - there are still significant overall energy benefits.

### 3.8 Evaluation of Different Combination Settings

With the parametric model, it is possible to evaluate every thinkable set of angle combinations. However, computational limitations require a discrete set of angles. In order to assess the influence of the chosen angle combinations on the performance of the ASF, various different combinations have been evaluated. In Figure 3.10, the energy savings of various simulation combinations are shown, compared to a fixed solar facade at a  $45^\circ$  altitude angle (a), as well as to a building without external shading (b). Variations include evaluations of using only one axis actuation (i.e. either a fixed azimuth or a fixed altitude angle), as well as using multiple angles for both altitude and azimuth actuation. The angles were always distributed equally between  $0^\circ$  and  $90^\circ$  or between  $-45^\circ$  and  $45^\circ$  for the altitude and azimuth variations, respectively. When using multiple angles, the maximum and minimum actuation angle was always included. For example, an analysis using three altitude and three azimuth angles used  $0^\circ$ ,  $45^\circ$  and  $90^\circ$  for the

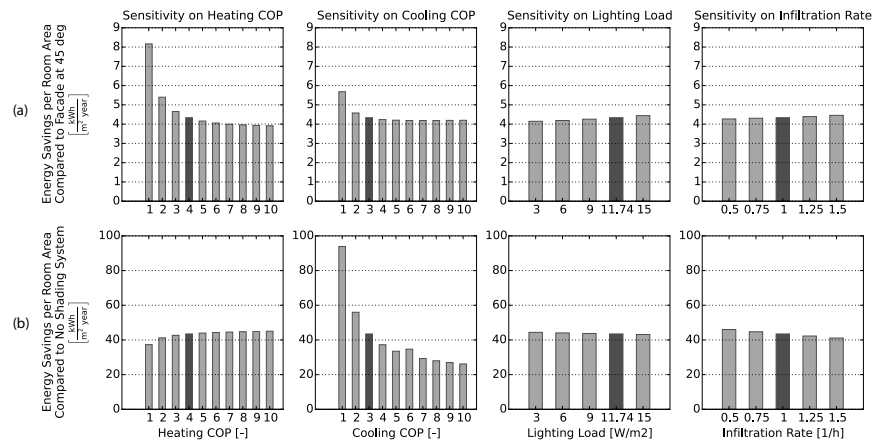


Figure 3.9: Sensitivity analysis of energy savings during one year. From left to right, sensitivities on heating COP, cooling COP, lighting load, and infiltration rate. The top row (a) shows the energy savings compared to a fixed solar facade at a  $45^\circ$  altitude angle, the bottom row (b) shows the energy savings compared to a room without shading or PV modules. The emphasized bar in every subplot corresponds to the basecase settings, all of them have the same height as they correspond to the same simulation.

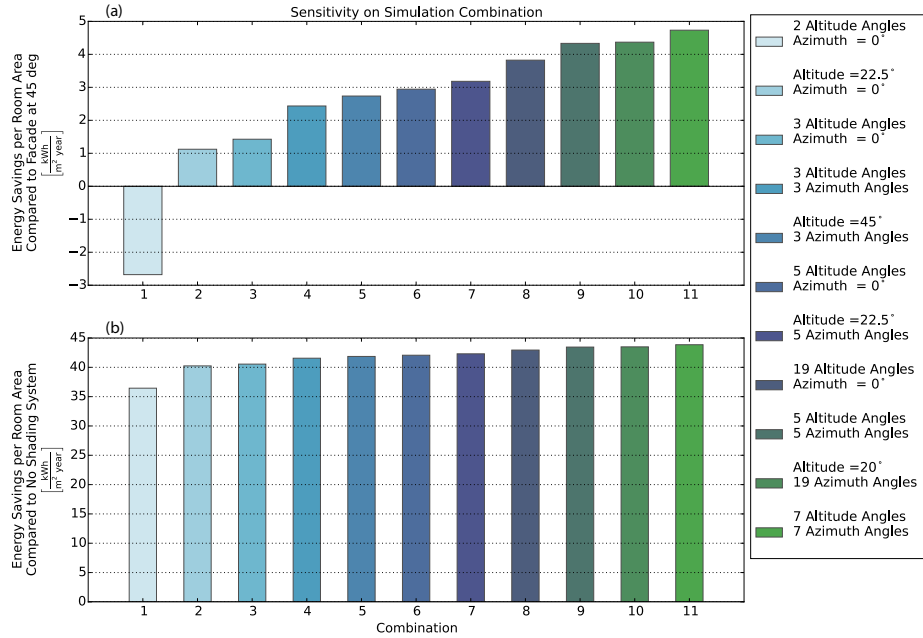


Figure 3.10: Comparison of different combination settings. (a) shows the energy savings compared to a fixed facade at a  $45^\circ$  altitude, (b) shows the savings in comparison to a building with no external shading.

altitude variations, while the azimuth variations would include the angles  $-45^\circ$ ,  $0^\circ$  and  $45^\circ$ . It can be seen that the more angles are used, the higher the energy savings become. However, with an increasing number of combinations comes a corresponding increasing amount of computation time. While an evaluation of five different combinations takes approximately four hours with the machine that was used, it goes up to 20 hours for the evaluation of 25 combinations or even 50 hours for the evaluation with 49 combinations. Higher energy savings will definitely be possible with the use of an increasing number of combinations, though the benefit of increasing the number of combinations will gradually go down to zero.

### 3.9 Potential of Independent Actuation

Independent actuation of the panels is one of the key advantages of the ASF that have to be closely evaluated. In order to quantize the potential of individual actuation, evaluations were performed by splitting the ASF into clusters. Due to computational limitations, especially on the radiation simulation, simplified geometries were used for the radiation evaluation. Ten panels in four rows with two clusters and eight panels in three rows with

three clusters were used, rather than the 50 panels of the reference case with one cluster. Furthermore, only the months of March, June, September, and December were evaluated. The two cluster evaluation was done for the reference case with five azimuth and five altitude angles. The evaluation with three clusters was done only for altitude variations, with 5 angles in each cluster. A visualization of the cluster comparison is shown in Figure 3.11. The left column details the comparison of two clusters against one cluster, whereas the right column shows the comparison of three clusters to one cluster. Figure 3.11a shows the net power use of the building for an average day of June, (b) depicts the corresponding power difference, and (c) details the average energy saving for the months of March, June, September and December. When looking at the power difference, it can be seen that the main benefit of using multiple clusters comes from deviations around noon and in the afternoon. This can be explained with the self-shading on the panels, as the facade has to optimise the longitudinal shading mainly in the afternoon (as described in Section 3.3). Therefore, the losses due to conflicts between cooling and PV can be reduced with the use of independent actuation. The comparison of the energy savings shows the impact on the conflicting energy yields. In the two cluster case, the energy benefits from heating and PV electricity are reduced, while cooling and lighting become more beneficial. The corresponding total energy demand could be reduced by approximately 1%. For three clusters, there are benefits for cooling, lighting and PV, though heating still brings some drawbacks. However, the corresponding total energy demand was reduced by 2.3%.

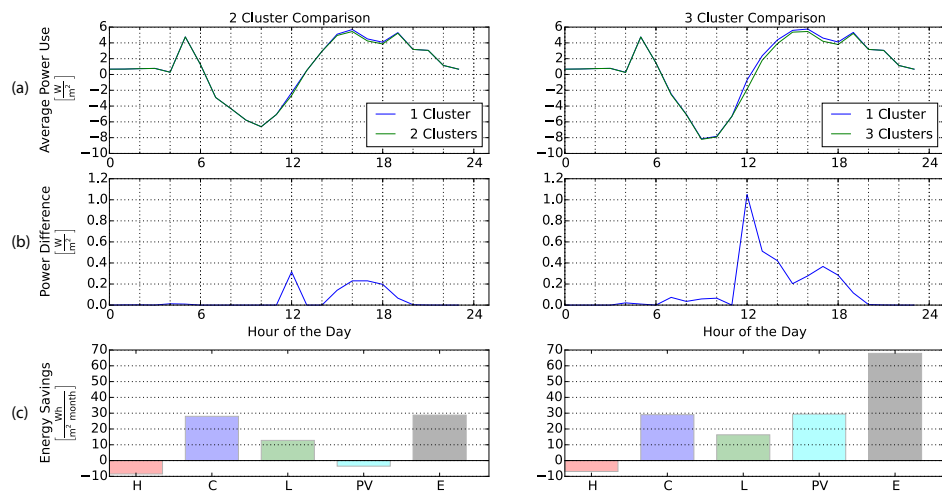


Figure 3.11: Cluster analysis of the ASF. The left column details the analysis with 2 clusters, whereas the right column corresponds to the 3 cluster analysis. (a) shows the average power use per room area for the month of June, (b) details the corresponding power difference, and (c) visualizes the total energy savings, averaged for the months of March, June, September and December.

## Chapter 4

# Conclusions

The work in this thesis presents a methodology to simultaneously evaluate PV electricity production and building energy demand of photovoltaic modules as adaptive building shading systems. A parametric model was created, to easily evaluate numerous different influences and designs, and a case study was done for the adaptive solar facade project (ASF). It was possible to find the optimising angles for heating, cooling, and lighting demand as well as for PV electricity production. Furthermore, the optimising angles that minimise the overall energy use were found. When combining the building energy with the PV electricity production, it could be shown that the ASF is able to generate more electricity than is used by the building for most sunlit hours.

The optimisation for PV electricity production was of particular importance. It was possible to show that sun-tracking does not optimise the PV power output. While sun-tracking simply follows the sun angles, the optimising algorithm yields the positions that correspond to the highest electricity output by finding the optimum mediation between maximising radiation and minimising longitudinal shading on the panels.

Also very important is the cooling performance of the ASF. The optimisation for PV, however, yields a good cooling demand performance. Heating and lighting, on the other hand, are not as important for the performance of the ASF, as they become most dominant at hours where there is no or little sun. Nevertheless, the heating and lighting also show benefits with the overall optimisation. Of course, these results strongly depend on the building system parameters. With a lower efficiency of heating, cooling or lighting, the corresponding energy demand will become significantly more important in the optimisation and the control in general. For the chosen base case, the optimisation was able to yield energy savings of 9% compared to a fixed solar facade at the optimum angle configuration, and the PV electricity production compensates for 41% of the building energy demand.

Furthermore, various parameters and their influence on the overall per-

formance of the system were analysed. Simulations done with different building orientations showed that the ASF performs best on a south-east facing facade due to increased cooling benefits. The most electricity, however, is generated from a south facing facade. Furthermore, south-west and west facing facades perform better with PV cells laid out parallel to the upper left edge of the panel, whereas south-east and east facing facades need the cells oriented the opposite way, i.e. parallel to the upper right edge.

Location evaluations were done for Helsinki, Zurich, Madrid and Cairo. Because of the significantly higher solar insolation and the warmer climate, the ASF performs best for the sunny regions of Madrid and Cairo. The highest PV electricity production was achieved for Madrid, this is because of the altitude angles of the sun, which are higher in Cairo and therefore generate increased self-shading on the panels.

A sensitivity evaluation of the building system parameters showed that heating and cooling COPs strongly influence the performance of the ASF, whereas lighting and infiltration rate do not have a very strong effect on the performance.

Evaluations of the number of simulation combinations showed that the discrete optimisation becomes more beneficial with an increasing number of evaluated combinations. Naturally the use of a smaller step size yields more accurate results of the optimisation.

Finally, the potential of independent actuation was analysed with simplified simulations using two and three clusters of independently moving panels. It was possible to show that with two clusters, the overall benefit increased by 1%, whereas for three clusters, it would rise up to 2.3%.

In summary, the following factors may be taken into consideration for future ASF designs:

- PV electricity production and cooling energy demand strongly influence the ASF performance.
- Sun-tracking does not yield the maximum electricity production, as it does not minimise longitudinal shading.
- An ASF performs best at a south or south-east facing facade.
- PV cells should be oriented parallel to the upper left edge for west and south-west facing facades, whereas the cells should be oriented parallel to the upper right edge for east and south-east facing facades.
- The energy benefit of an ASF is particularly large in warm and sunny regions, such as Madrid and Cairo.
- With low cooling COPs, the energy savings of an ASF increase substantially.

This work ultimately presents a methodology for the planning and optimisation of sophisticated adaptive BIPV systems. The dynamic PV integrated shading system has clear advantages to a static system as it can adapt itself to the external environmental conditions. This enables it to orientate itself to the most energy efficient position. Through various simulations, it was possible to demonstrate and quantize the benefits of such a system, as well as suggesting factors that should be taken into account for future design considerations and further system performance evaluations.

## **Chapter 5**

### **Outlook**

While the results of this thesis are promising, further research must be done on many aspects. Optimisation algorithms must be found to determine the best state of the system with individual actuation while taking into account all influences. The optimisation algorithms could be included into the control of a real system so that it can be at the optimum position at all times. Influences of user satisfaction, behaviour, and comfort have to be evaluated as well, and must ultimately be included in the optimum control methods. Furthermore, the PV panels must be connected into strings for the evaluation and the influence of bypass diodes should be included. In order to evaluate the building performance in more detail, the methodology needs to be changed to calculate building energy demand for single hours, taking into account the inertia of the system. Also, the energy needed for the actuation of the panels should be modelled and included into the optimisation to determine whether the energy savings from the improved position are higher than the actuation energy needed to get to that position. Other influences that can be evaluated in more detail include the reflectance of the panels, the ventilation, or the user interaction. In order to increase the accuracy of the simulations, an iterative optimisation algorithm could be developed and implemented in the future, in order to increase the accuracy of the simulation results. Finally, even though life cycle analysis was done before for this project, it should now be done again with the enhanced energy performance results, and could ultimately even be integrated into the simulation environment.

## Appendix A

# Usage of Simulation Environment

This appendix chapter describes the usage of the simulation environment. It provides essentially the same content as the github wiki that can be found at

[https://github.com/architecture-building-systems/ASF\\_Simulation/wiki](https://github.com/architecture-building-systems/ASF_Simulation/wiki).

First, a description on how to get the simulation environment and what tools must be installed is given. Then, the main files that run the evaluations are described in detail. Finally, a step-by-step guide leads through the detailed usage of the simulation environment.

### A.1 Get ASF\_Simulation Folder

In order to use the ASF simulation framework, one can either download the .zip file and unpack the folder or use the following commands within git:

#### A.1.1 Git Set-Up

In the working directory, type:

```
git init
```

Then checkout the repository:

```
git clone https://github.com/architecture-building-systems/ASF_Simulation.git
```

To download the files, type:

```
git pull
```

## A.2 Installation Guides

This section describes, what programs and add-ons are needed and where they can be downloaded.

### A.2.1 Installing Rhino

Rhino can be downloaded from <https://www.rhino3d.com/download>. At least Rhino 5 is required, an appropriate licence must be available.

### A.2.2 Installing Grasshopper

Open Source add-on for Rhino, that can be found on:

<http://www.grasshopper3d.com/page/download-1>

#### Grasshopper Add-Ons

- GhPython: Enables the use of Python scripts within Grasshopper  
<http://www.food4rhino.com/project/ghpython?etx>
- DIVA/VIPER: Connects Grasshopper to EnergyPlus  
<http://diva4rhino.com/>  
+ The Zuerich-Kloten weather file must be added to *C:/DIVA/WeatherData*
- Hoopsnake: For looping grasshopper scripts  
<http://www.food4rhino.com/project/hoopsnake?etx>
- Ladybug/Honeybee: Thermal and radiation simulations  
[https://github.com/mostaphaRoudsari/ladybug/blob/master/resources/Installation\\_Instructions.md](https://github.com/mostaphaRoudsari/ladybug/blob/master/resources/Installation_Instructions.md)
- Human: Some additional functions for GH  
<http://www.food4rhino.com/project/human?etx>
- Mesh Tools: Create and customise meshes within Grasshopper  
<http://www.food4rhino.com/project/meshedittools>

### A.2.3 Installing Python

Anaconda is recommended as it is easy to create virtual environments and manage python:

<https://www.continuum.io/downloads>

For manual installation, the following guide can be used:

<http://www.lowindata.com/2013/installing-scientific-python-on-mac-os-x/>

The packages numpy, scipy, matplotlib and ipython have to be included in thy python installation.

## A.3 Grasshopper Simulations

Once everything described in Section A.2 is installed, simulations can be run. This section describes the different parts of the grasshopper simulation environment, given in the *main.gh* simulation script. In order to open the Grasshopper script, one can open an empty rhino file and type ‘grasshopper’ in the command line. The *main.gh* file can now be opened from the folder *Simulation\_Environment* in grasshopper.

### A.3.1 General Description of *main.gh*

GhPython scripts generate the geometry of the ASF of every possible configuration. The script then loops through every configuration and runs an EnergyPlus simulation and a Ladybug simulation on every geometry for each hourly time step. Special attention has to be given to the sections in the script which have a red frame, these sections should be checked before every simulation, to make sure that it is running correctly. Furthermore, one has to be aware of the places the results are stored, and the instructions given on how to save the data should be closely followed.

### A.3.2 Set Geometry

User Interaction on general geometry and simulation inputs.

#### ASF Simulation Inputs

Angles, number of clusters and the desired grid point size that will be used for the simulation are set in this section. The desired grid point size is only relevant for the ladybug analysis.

#### Geometry Inputs

General inputs for the room and the ASF geometry.

### A.3.3 Geometry Calculations

Processing of the geometry inputs, creates the geometry and saves inputs.

#### Save Inputs

Python script that saves ASF geometry and simulation inputs.

### Render the Building

GhPython script *Render\_Room* creates the building geometry for simulation. The room width, height, depth and glazing fractions of the front facade can be selected.

### Render the ASF

- **Generate Diamond Array:** Produces a matrix of coordinates of where a PV panel should exist
- **Combination Maker:** Determines the combination of PV panels. When running a simulation, **it must always be made sure that the right combination is connected** (either EplusComb or RadiationComb, framed in red)
- **Render Diamond Array:** Generates the geometry based off the chosen combination and array.

### A.3.4 EnergyPlus Simulation

In this section the EnergyPlus simulations are run.

### DIVA Interface Conversion

- Converts ASF panels into DIVA shading elements
- Converts all interior walls into adiabatic surfaces
- Converts the front wall to a facade element
- Converts the glazed section into a window element

### Run the Simulation

Run through the Viper interface. **It is important that the right settings are used.** Especially the weather file is subject to change. For the DIVA analysis, this can only be done in the Viper settings.

- Lx set point: variable (evaluations were done with a value of 300)
- Heating COP: variable (evaluations were done with a value of 4)
- Cooling COP: variable (evaluations were done with a value of 3)
- Lighting Load: variable (evaluations were done with the default value of  $11.74 \text{ W/m}^2$ )
- Infiltration: variable (evaluations were done with a value of 1/h)

- Fresh Air: variable (evaluations were done with a value of 0.016  $\frac{m^3}{s \cdot person}$ )

### Save Data

Python script that saves the DIVA data for post processing. The folder where it will be saved is set automatically in the script *set DIVA data path* to *Simulation\_Environment/data/grasshopper/DIVA/DIVA\_results*. **After a simulation finishes, the acquired data has to be moved to a separate folder with a unique name, which will be used for post processing.** Alternatively, the folder *DIVA\_results* can simply be renamed. It is good practice to also save a backup of the current *main.gh* file to this folder ([Ctr+Alt+s] saves a backup).

### A.3.5 Loop EnergyPlus

Uses hoopsnake to iterate through all possible configurations. It must be made sure that the hoopsnake algorithm is connected correctly.

### A.3.6 Set Weather File

The weather file used for the ladybug radiation analysis is set in this section. The desired .epw file must already be in the WeatherData folder and the full name of the weather file has to be input to the *weatherPath* Python script.

### A.3.7 Save Details of Weather File

The weather file that was specified is read and relevant information on the sun position and the temperature is saved to the folder *Simulation\_Environment/data/geographical\_location*. If a new weather file is used, the main.py file has to be run in *initialize* mode to prepare the data for further use with grasshopper. It must be made sure that the component *Ladybug\_SunPath* is enabled when a new weather-file is introduced.

### A.3.8 Loop LadyBug

In this section, Ladybug is looped according to the specified angle combinations and for relevant hours (see Section A.3.9)

### A.3.9 Set Evaluation Period

Analysis period is set according to the loop number and the auxiliary data on the sun positions.

### A.3.10 Ladybug Solar Analysis

First of all, one has to let ladybug fly. For this the ladybug\_ladybug component has to be put onto the GH screen. This component has to run first, if there still are warnings that you first have to let ladybug fly, click on the component and press CTRL+B, then disable and enable again components that show the warning. This ensures, that the ladybug\_ladybug component runs first.

#### Create Mesh for Radiation Analysis

Creates a mesh of the ASF for the radiation analysis according to the desired grid point size. The normals of the ASF geometry are flipped so that they face away from the building.

#### Create Sky Matrix

In the selectSkyMtx component, it is possible to either choose a specific hour of the year or a period of time, which can be chosen with the Analysis Period component. **WARNING: This component is not working correctly in the current version of ladybug.** The bug has been found, fixed, and reported to the developers:

<https://github.com/mostaphaRoudsari/ladybug/issues/233>

#### Calculate Radiance on Panels

Calculates the radiance on a specified geometry. The simulation is done for the chosen settings given by the SelectSkyMtx component. **Toggle runIt to start the evaluation,** this can take up to 20 seconds on a fast computer.

#### Sky Dome for reference

This component creates sky domes, that show where the radiation is coming from.

### A.3.11 Save Radiation Results

The detailed radiation results are saved to a .csv file with a C# script. The results are saved to the folder *Simulation\_Environment/data/grasshopper/LadyBug/radiation\_results*. It should be made sure that this folder is empty before starting a simulation, because otherwise there might be *leftover* data, which will fill up space without being used. The *copyLayoutAndComb* component copies the file generated in the *Geometry Calculations* section and also saves it to the *radiation\_results* folder for convenience. **After a simulation finishes, the acquired data has to be moved to a separate folder with a unique name, which will be used for post processing.**

Alternatively the *radiation-results* folder can be renamed. It is good practice to also save a backup of the current *main.gh* file to this folder ([Ctr+Alt+s] saves a backup).

## A.4 Python Evaluation

The data that was previously generated by the *main.gh* script is read in by the *main.py* file and post-processed to output several graphs, aggregated data, and a *summary.csv* file.

### A.4.1 Main Python File

The *main.py* file is the main file for the python evaluation. There are two modes: *initialize* and *post-processing*. If an evaluation is done for the first time for a specific location, it must first run in *initialize* mode, otherwise it can be run directly in *post-processing* mode. At the beginning of the script, there is a user interaction section. When starting an evaluation, a user must go through this section to make sure everything is set as wished. All variables are described in detail right before they are defined.

### A.4.2 Compare Results

The file *compareResults.py* can be used to generate various plots on comparing simulation results. The corresponding result folders must be set manually, and adjustment might be needed in the script.

### A.4.3 Post-Process Sun Tracking

The file *PostProcessSunTracking.py* can be used to compare a sun-tracking approach to an optimized solution. In order to run this script, the corresponding optimization results must be available and the folders that will be compared have to be manually set.

### A.4.4 Create Further Visualisations

With the file *createFiguresAfterMain.py*, additional plots can be generated that visualize the simulation results.

### A.4.5 Auxiliary Files

The *aux\_files* folder contains all auxiliary files that are needed for the post-processing and the optimisation. It is recommended to go through an optimisation-run step-by-step, in order to clearly understand how the simulation works.

## A.5 First Time Set-Up of a Simulation

All the files that are necessary to perform simulations of the ASF are in the folder *Simulation\_Environment*. There are two main simulation files, one for grasshopper, the other one for the python part of the simulation (*main.gh*, *main.py*). In order to get started with simulations, the following steps have to be taken to generate the auxiliary files that are needed:

1. Open the *main.gh* file.
2. Assign the desired weather file that will be used for the radiation simulation in the section *Set Weather File*.
3. Make sure that the component *Ladybug\_SunPath* is enabled in the section *Save details of weather file*. A new folder in *Simulation\_Environment/data/geographical\_location* with the name of the location and information on temperature and the sun position will now be created.
4. Open the *main.py* file.
5. In the *user interaction* section, the *mainMode* must be set to *initialize* and the *geoLocation* must be set to the folder that was generated in grasshopper (for the zurich-kloten epw file, the corresponding folder is called *Zuerich-Kloten*). The other options do not yet require any change, as they are only important for the post-processing mode.
6. Run the *main.py* script. Be aware that the first time the file is run, it will take some time, as the lookup-table for the pv-electricity-generation needs to be generated first.
7. Once the *main.py* script has finished without errors, the *Ladybug\_SunPath* component in the section *Save details of weather file* of the *main.gh* script can be disabled again, as it is no longer needed. This will speed up the initialization of grasshopper when restarting it.

Now, simulations can be run with grasshopper, as described in the following section.

## A.6 Run Grasshopper Simulations

After carefully following the instructions given in Sections A.1, A.2, and A.5, simulations can now be run using grasshopper by taking the steps described in this section.

### A.6.1 General Simulation Set-Up

1. Open *main.gh*
2. Make sure the *run* switch in the *E+ Simulation* section as well as the *\_runIt* switch in the *Ladybug Solar Analysis* section are set to False
3. Set the building geometry and the facade geometry for the simulation in the section *Set Geometry*

### A.6.2 Run a LadyBug Radiation Simulation

1. Set the weather file in the section *Set Weather File* (If you want to use a new weather file, follow the instruction given in Section A.5)
2. Reset HoopSnake in the section *Loop Lady Bug*
3. Go to the folder *ASF\_Simulation/Simulation\_Environment/data/grasshopper/LadyBug/radiation\_results* and make sure it is empty.
4. Connect *RadiationComb* to the *combination* input of the *Combination Maker V2* in the Section Geometry Calculations
5. Test loop hoopsnake and make sure the combinations are run as desired. It can be stopped by right clicking on hoopsnake and selecting *stop*.
6. Reset hoopsnake again.
7. Toggle the *\_runIt* input in the *Ladybug Solar Analysis* section to true.
8. Go again to the *radiation\_results* folder and see if the .csv file for the first iteration was created. Also look at the graphical output from Ladybug in the rhino scene, make sure everything is evaluated as desired.
9. If everything looks fine, start to loop hoopsnake again.
10. Check that the *LayoutAndCombinations.txt* file was created in the *radiation\_results* folder and look at the csv files to see if the results are reasonable.
11. Wait until the simulation is done. This step will generally take several hours, so it is a good idea to let it run over night.
12. When the simulation is over, the folder *radiation\_results* has to be renamed to have a unique name, typical for the simulation, such as *Radiation\_Kloten\_5x\_1y\_2clust\_SE*.
13. Turn off the radiation analysis (set *\_runIt* to False). This will automatically create a new and empty *radiation\_results* folder.

14. Save a backup of the *main.gh* file ([CTR+ALT+s]) and move it to the folder where the results are saved.

### A.6.3 Run an EnergyPlus Building Simulation

1. Set the desired weather file and other options in the Viper component settings in the section *E+ Simulation*
2. Set all other options in this section.
3. Connect *EplusComb* to the *combination* input of the *Combination Maker V2* component in the *Geometry Calculations* section.
4. Loop hoopsnake in the *Loop E+* section while looking at the rhino scene to make sure the desired combinations will be evaluated.
5. Reset hoopsnake in the *Loop E+* section.
6. Turn the run input toggle in the *E+ Simulation* section to true.
7. Go to the folder *ASF\_Simulation/Simulation\_Environment/data/grasshopper/DIVA/DIVA\_results* and check the *LayoutAndCombinations.txt* file as well as the first iteration.
8. Check the output of the VIPER component in the *E+ Simulation* section, there should be no errors and no warnings.
9. When everything looks fine, loop hoopsnake in the *Loop E+* section.
10. Check the rhino scene and the result files to make sure everything is working correctly while looping.
11. Rename the *DIVA\_results* folder to a unique name, such as *DIVA\_Kloten\_5x\_1y\_2clust\_SE*.
12. Turn the *run* input of VIPER to False. This will create a new, empty *DIVA\_results* folder.
13. Save a backup of the *main.gh* file ([CTR+ALT+s]) and move it to the folder where the results are saved.

## A.7 Run Python

Once the grasshopper simulations (Section A.6) are finished, the results can be post-processed in order to visualize the data, find the optimum angle combinations as well as the corresponding energies.

1. Open *main.py*

2. Set all the post-processing options in the user interaction section (each variable is described in detail before its definition)
3. Run *main.py* (you can press F5)
4. A folder with the corresponding optimization results will be created in *ASF\_Simulation/Simulation\_Environment/results*. The created folder is named with the date and time of the simulation start.
5. Rename the result folder
6. Done

# Appendix B

## Further Results

### B.1 Building Energy Analysis

As the building energy results are available for every hour of the year, they can be visualised in greater detail than the overall results that include the PV electricity production given in Section 3.1.

The optimal configurations of the ASF can be visualised using carpet-plots. For a classical building analysis this was done for every hour of the year. Figures B.1 and B.2 show the optimizing altitude and azimuth angles for heating, cooling, lighting and total building energy demand. In figure B.1, darker colours represent closed positions, whereas brighter colours correspond to open positions. To optimize heating and lighting, open positions (corresponding to large altitude angles) are favourable, cooling is optimized by using closed positions (corresponding to small altitude angles). The overall optimized solutions follow the corresponding patterns at the hours of importance. The azimuth angles in figure B.2 correspond to the deviation from the facade normal. For a south facing facade, this means an angle with a positive sign represents the panels facing towards south-east (bright colours), whereas negative angles represent the panels facing towards south-west (dark colours). It can be seen that for heating and lighting, the facade takes positions that let the sun in, whereas for cooling the facade follows a sun-tracking pattern which prevents radiation to enter the room.

Figure B.3 depicts the corresponding energy demand of the building for the whole year corresponding to the optimum positions presented in figures B.1 and B.2. It can be seen that heating is most needed during the winter and in the morning, whereas cooling is mainly apparent in summer afternoons. Lighting on the other hand is most important in the evenings and at times where there is not much sun. In the combined plot, this behavior can be seen clearly as well, the main overlaps of different building energy consumptions take place during winter between heating and lighting in the morning and in the evening, and between cooling and lighting during

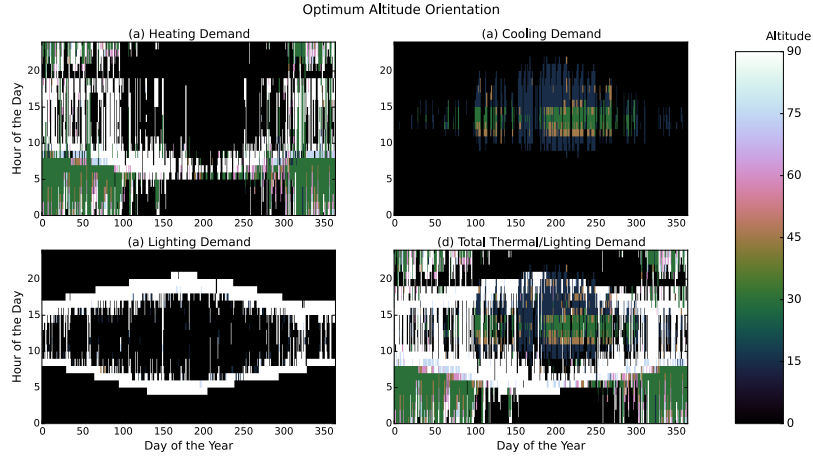


Figure B.1: Carpet plots detailing the optimal altitude angles to minimise the (a) heating demand, (b) cooling demand, (c) lighting demand, and (d) total building energy demand. Darker colours represent closed positions, whereas brighter colors correspond to open positions. To optimize heating and lighting, open positions are favorable, cooling is optimized by using closed positions.

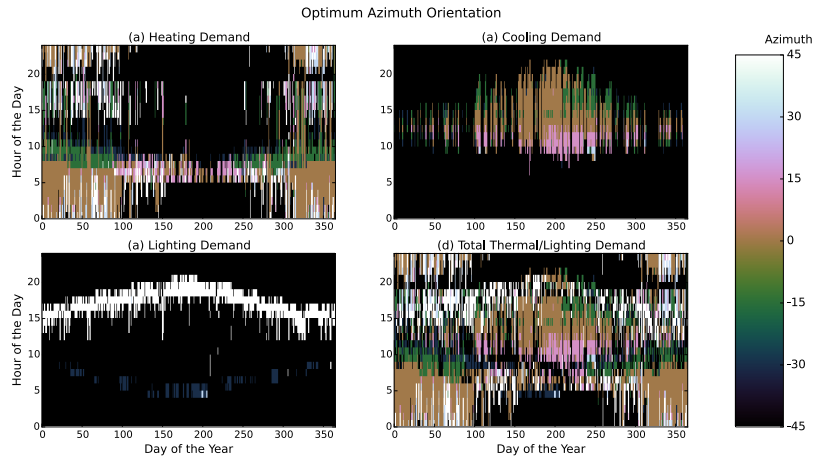


Figure B.2: Carpet plots detailing the optimal azimuth angles to minimise the (a) heating demand, (b) cooling demand, (c) lighting demand, and (d) total building energy demand. Cooling is minimized by blocking the sun, whereas lighting and heating are minimized by opening the facade to let the insolation in.

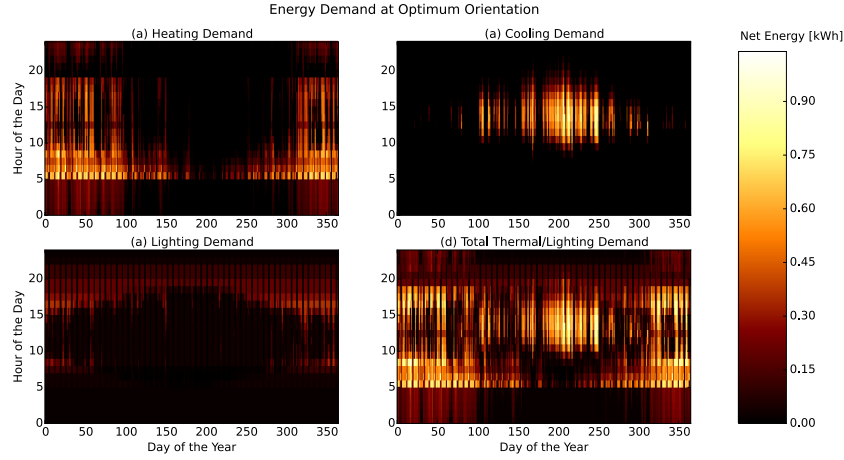


Figure B.3: Carpet plots detailing the energy consumption during every hour of the year for the (a) heating demand, (b) cooling demand, (c) lighting demand, and (d) total building energy demand.

summer evenings.

## B.2 Further Visualisations of Radiation and PV results

The results of Sections 3.1 and 3.3 were further visualised as can be seen in the following. Figure B.4 compares the angles that optimise PV electricity production with the angles that optimise the total radiation on the panels. The difference in the optimising angles can nicely be seen when comparing them side by side. While the radiation optimisation yields a symmetric pattern, the PV electricity production uses different angles, mainly in the afternoon. Figures B.5 and B.6 correspond to the summarising Figure 3.5, but also show the actual difference in the power production and the efficiency, respectively.

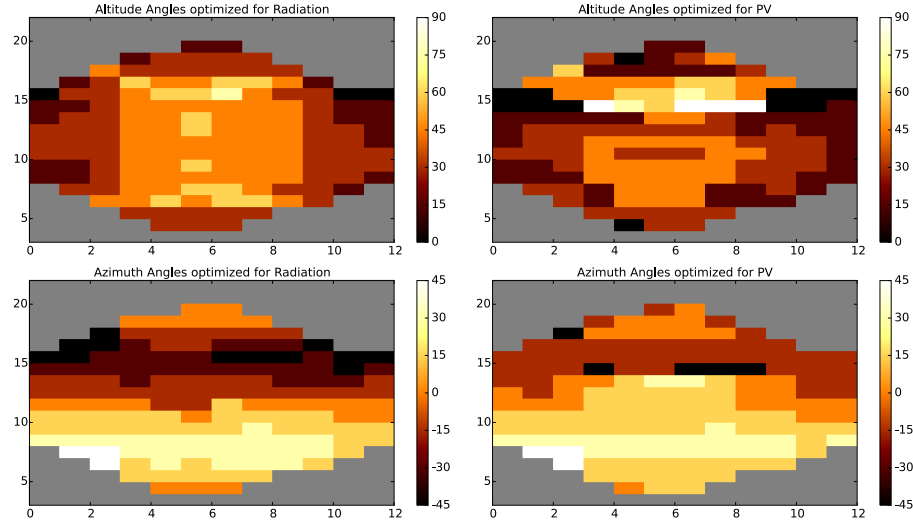


Figure B.4: Angle visualisations, that optimise the altitude (top) and azimuth (bottom) angles for radiation (left) and PV electricity production (right). While the Radiation optimisation yields a symmetric pattern, the PV electricity optimisation deviates from the pattern that optimises the radiation in order to minimise longitudinal shading on the panels.

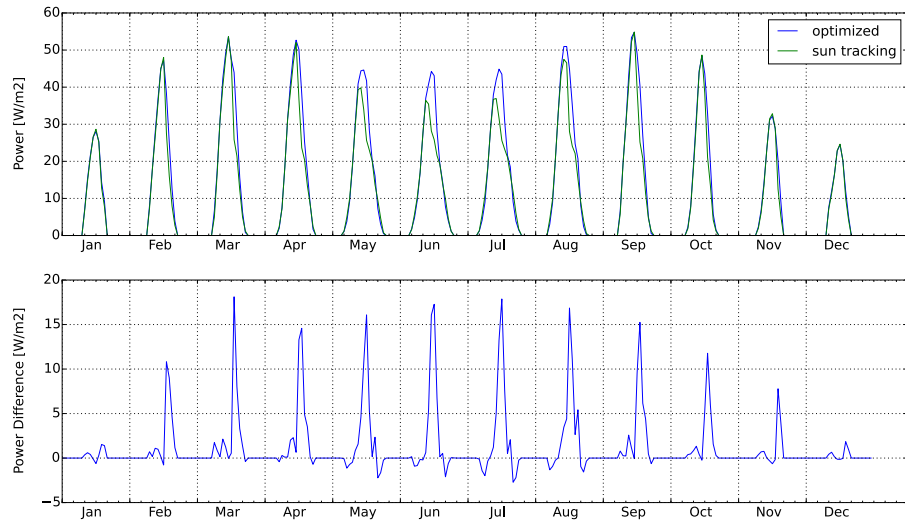


Figure B.5: Comparison of PV electricity production with sun tracking to optimised solution. Top: Average power output for every month of the year. Bottom: Corresponding power difference. The difference is especially high during noon and in the afternoon.

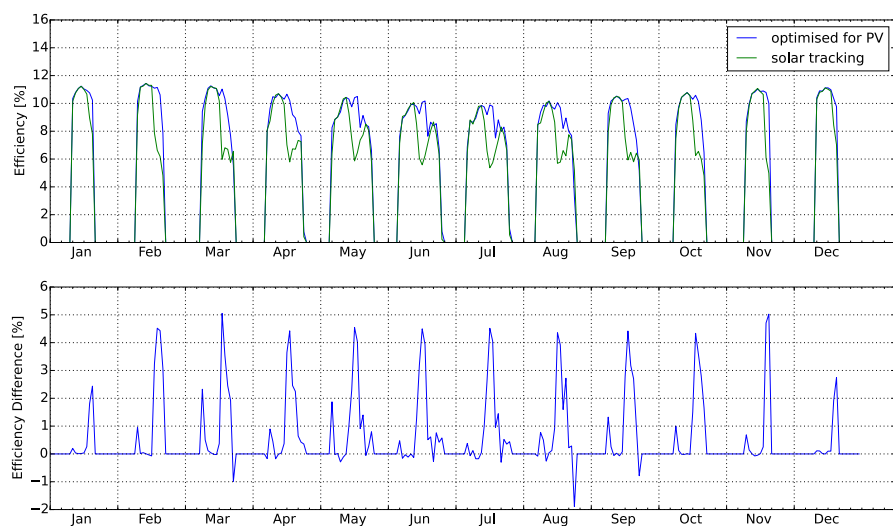


Figure B.6: Comparison of PV efficiency with sun tracking to optimised solution. Top: Average efficiency for every month of the year. Bottom: Corresponding efficiency difference. The difference is especially high during noon and in the afternoon.

### B.3 Tradeoffs Between Different Optimisation Strategies

In order to visualize the tradeoffs between the different optimisation strategies, figures were created that show the influence of the different optimisation strategies on heating (figure B.7), cooling (figure B.8), lighting (figure B.9), PV electricity (figure B.10), total building energy (figure B.11) and net energy (figure B.12). Optimisation strategies were evaluated for heating (H), cooling (C), lighting (L), photovoltaic (PV), building energy demand (HCL), net energy demand ( $E_{tot}$ ), a combination of PV and cooling, and a fixed facade at a  $45^\circ$  altitude angle. The results from sections 3.2 and 3.4 can be visualized here in more detail. It can clearly be seen, that while the cooling demand and the PV electricity production are strongly influenced by the actuation and the optimisation strategy, the lighting and heating have less fluctuations within the energy performance.

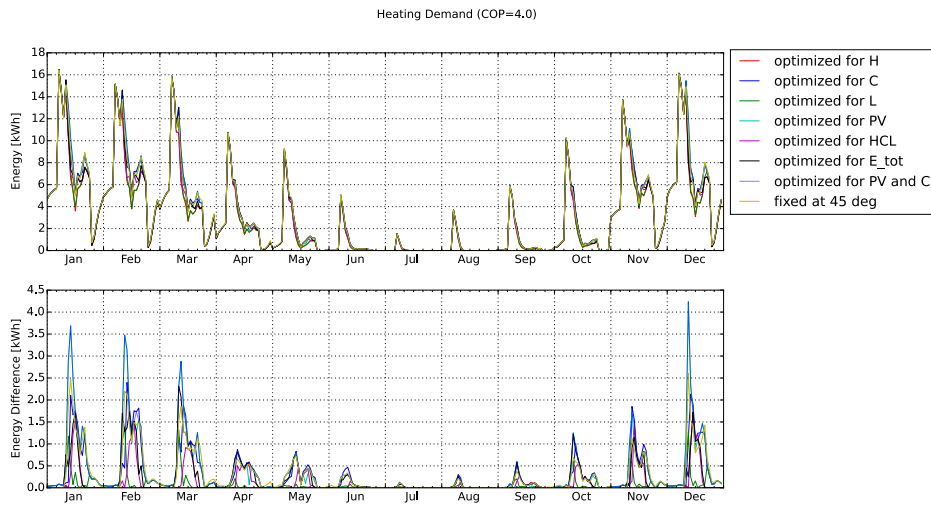


Figure B.7: Influence of optimisation strategy on heating demand. Top: Energy demand of heating in dependence of optimisation strategy. Bottom: Corresponding difference to heating optimisation.

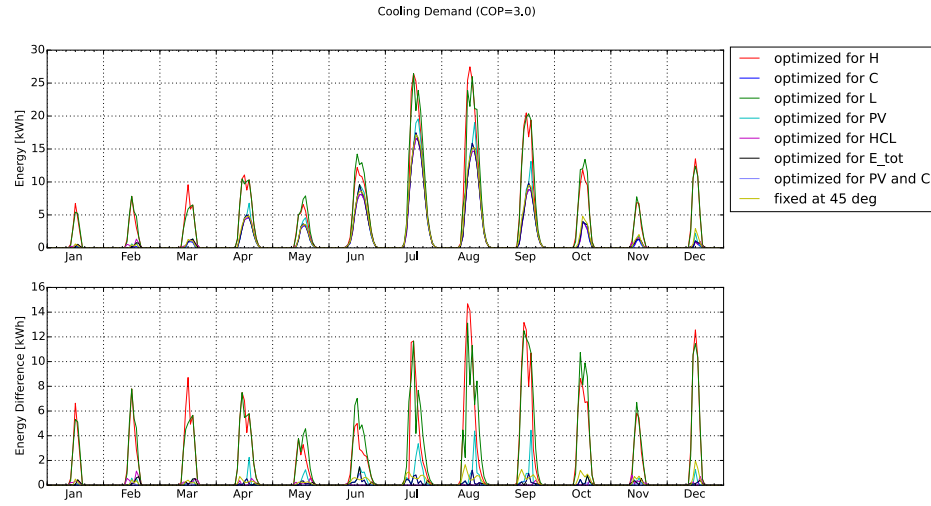


Figure B.8: Influence of optimisation strategy on cooling demand. Top: Energy demand of cooling in dependence of optimisation strategy. Bottom: Corresponding difference to cooling optimisation.

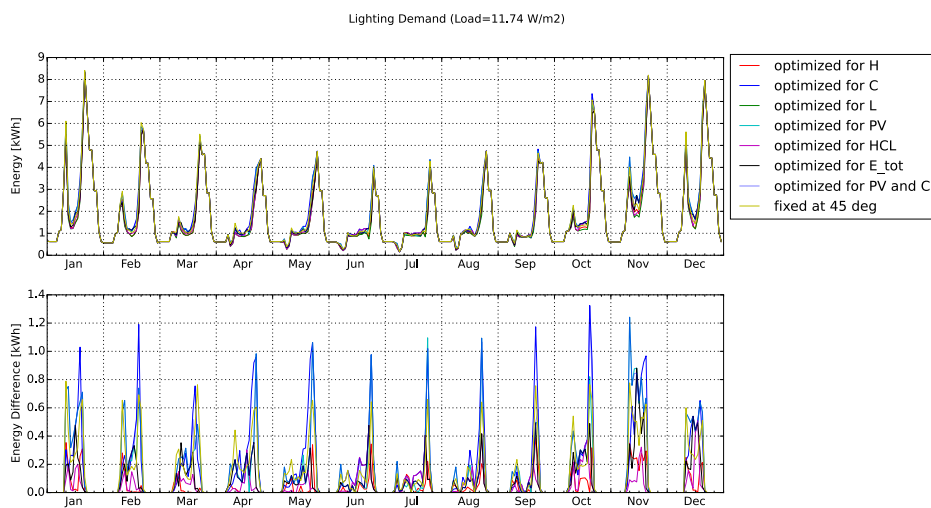


Figure B.9: Influence of optimisation strategy on lighting demand. Top: Energy demand of lighting in dependence of optimisation strategy. Bottom: Corresponding difference to lighting optimisation.

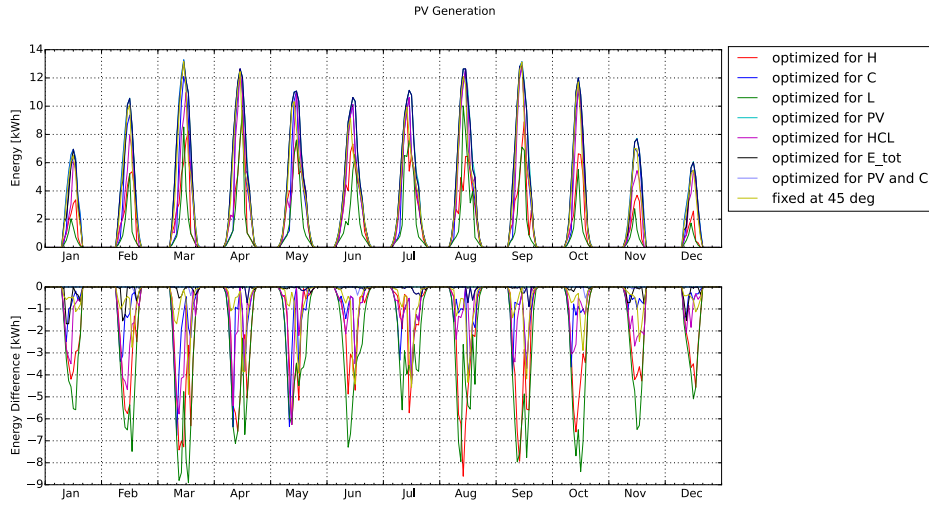


Figure B.10: Influence of optimisation strategy on PV electricity production. Top: Energy demand of PV electricity production in dependence of optimisation strategy (negative because production corresponds to a negative demand). Bottom: Corresponding difference to PV electricity optimisation.

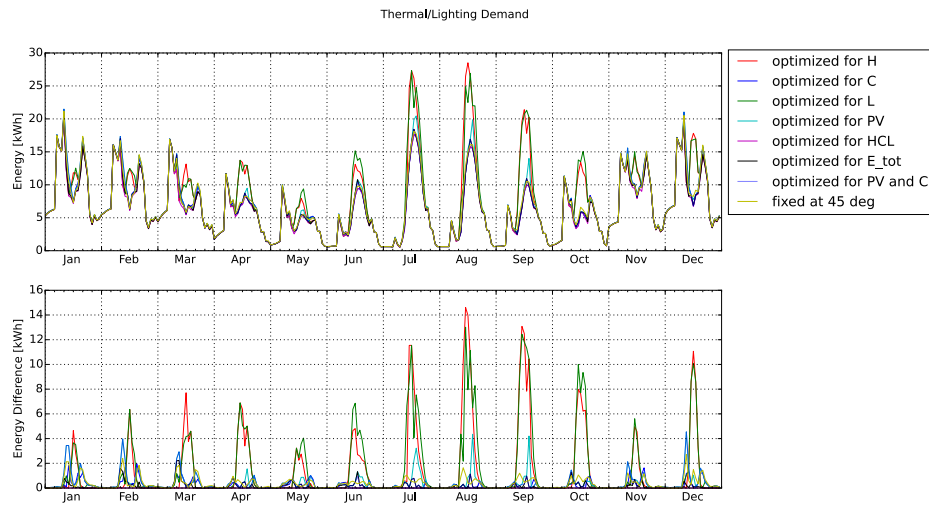


Figure B.11: Influence of optimisation strategy on building energy demand. Top: Building energy demand in dependence of optimisation strategy. Bottom: Corresponding difference to building energy demand optimisation.

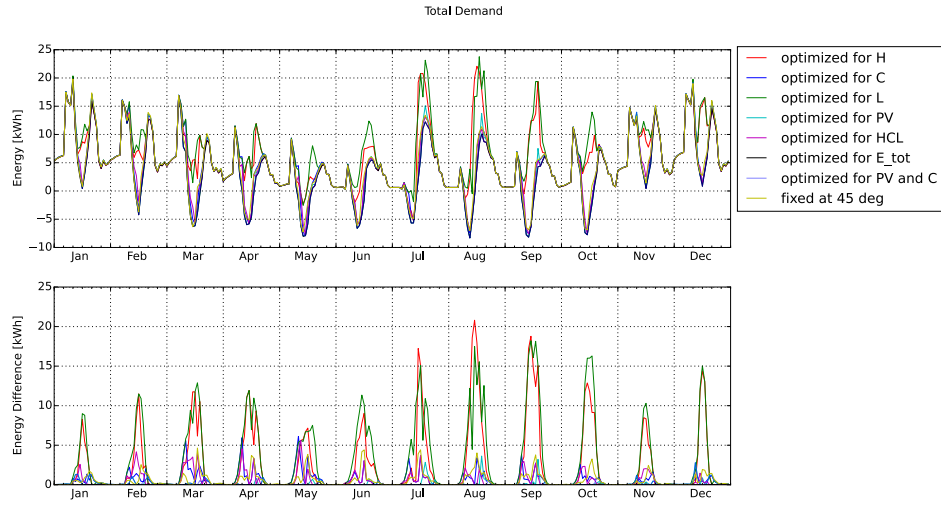


Figure B.12: Influence of optimisation strategy on net energy demand including PV electricity production. Top: Net energy demand in dependence of optimisation strategy. Bottom: Corresponding difference to overall optimisation.

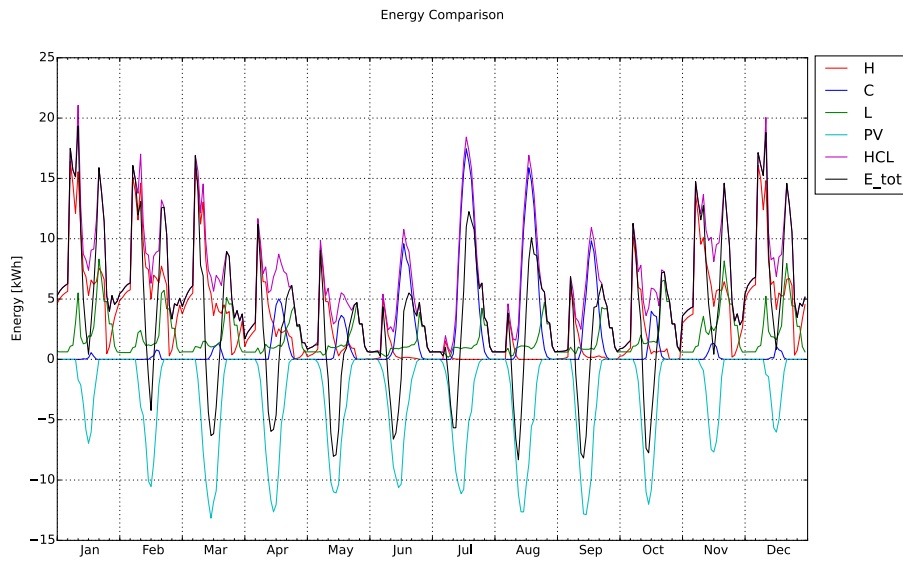


Figure B.13: Energy demand distribution at overall optimization.

# Bibliography

- [1] Z. Nagy, B. Svetozarevic, P. Jayathissa, M. Begle, J. Hofer, G. Lydon, A. Willmann, and A. Schlueter. The adaptive solar facade: From concept to prototypes. *Frontiers of Architectural Research (in press)*, 2016.
- [2] Fifth assessment report, mitigation of climate change. *Intergovernmental Panel on Climate Change*, pages 674–738, 2014.
- [3] P. Defaix, W. van Sark, E. Worrell, and E. de Visser. Technical potential for photovoltaics on buildings in the eu-27. *Solar Energy*, 86(9):2644–2653, 2012.
- [4] M. Raugei and P. Frankl. Life cycle impacts and costs of photovoltaic systems: current state of the art and future outlooks. *Energy*, 34(3):392–399, 2009.
- [5] R. Loonen, M. Trčka, D. Cóstola, and J. Hensen. Climate adaptive building shells: State-of-the-art and future challenges. *Renewable and Sustainable Energy Reviews*, 25:483–493, 2013.
- [6] D. Rossi, Z. Nagy, and A. Schlueter. Adaptive distributed robotics for environmental performance, occupant comfort and architectural expression. *International Journal of Architectural Computing*, 10(3):341–360, 2012.
- [7] R. Loonen, F. Favino, J. Hensen, and M. Overend. Review of current status, requirements and opportunities for building performance simulation of adaptive facades. *Journal of Building Performance Simulation (in press)*, 2016.
- [8] M. Nielsen, S. Svendsen, and L. Jensen. Quantifying the potential of automated dynamic solar shading in office buildings through integrated simulations of energy and daylight. *Solar Energy*, 85(5):757–768, 2011.
- [9] L. Sun and H. Yang. Impacts of the shading-type building-integrated photovoltaic claddings on electricity generation and cooling load component through shaded windows. *Energy and Buildings*, 42(4):455 – 460, 2010.

- [10] L. Sun, L. Lu, and H. Yang. Optimum design of shading-type building-integrated photovoltaic claddings with different surface azimuth angles. *Applied Energy*, 90(1):233 – 240, 2012.
- [11] M. David, M. Donn, F. Garde, and A. Lenoir. Assessment of the thermal and visual efficiency of solar shades. *Building and Environment*, 46(7):1489 – 1496, 2011.
- [12] M. Mandalaki, K. Zervas, T. Tsoutsos, and A. Vazakas. Assessment of fixed shading devices with integrated pv for efficient energy use. *Solar Energy*, 86(9):2561–2575, 2012.
- [13] M. Mandalaki, S. Papantoniou, and T. Tsoutsos. Assessment of energy production from photovoltaic modules integrated in typical shading devices. *Sustainable Cities and Society*, 10:222 – 231, 2014.
- [14] M. Mandalaki, S. Papantoniou, and T. Tsoutsos. Assessment of energy production from photovoltaic modules integrated in typical shading devices. *Sustainable Cities and Society*, 10:222–231, 2014.
- [15] S. Yoo and H. Manz. Available remodeling simulation for a bipv as a shading device. *Solar Energy Materials and Solar Cells*, 95(1):394–397, 2011.
- [16] P. Jayathissa, Z. Nagy, N. Offedu, and A. Schlueter. Numerical simulation of energy performance and construction of the adaptive solar facade. *Proceedings of the Advanced Building Skins*, 2:52–62, 2015.
- [17] S. Freitas and M. Brito. Maximizing the solar photovoltaic yield in different building facade layouts. *EU PVSEC (2015)*, 2015.
- [18] J. Hofer, A. Groenewolt, P. Jayathissa, Z. Nagy, and A. Schlueter. Parametric analysis and systems design of dynamic photovoltaic shading modules. *Energy Science & Engineering*, 4(2):134–152, 2016.
- [19] Rhinoceros v5. <https://www.rhino3d.com/>, 2015.
- [20] Grasshopper - algorithmic modeling for rhino. <http://www.grasshopper3d.com/>, 2015.
- [21] D. Crawley, L. Lawrie, C. Pedersen, and F. Winkelmann. Energy plus: energy simulation program. *ASHRAE journal*, 42(4):49–56, 2000.
- [22] J. Mitchell J. Duffie N. Duffie T. Freeman S. Klein, W. Beckman. *TRNSYS 16 - A Transient System Simulation Program*. Solar Energy Laboratory, University of Wisconsin–Madison, 2006.
- [23] Diva for rhino. <http://diva4rhino.com/>.

- [24] M. Roudsari, M. Pak, A. Smith, and G. Gill. Ladybug: a parametric environmental plugin for grasshopper to help designers create an environmentally-conscious design. In *Proceedings of the 13th International IBPSA Conference Held in Lyon, France Aug*, 2013.
- [25] G. Ward. The radiance lighting simulation and rendering system. In *Proceedings of the 21st annual conference on Computer graphics and interactive techniques*, pages 459–472. ACM, 1994.
- [26] A. Mermoud and T. Lejeune. Performance assessment of a simulation model for pv modules of any available technology. In *Proceedings of the 25th European Photovoltaic Solar Energy Conference*, Munich, 2010.
- [27] R. Ross and M. Smokler. *Flat-Plate Solar Array Project: Final report: Volume 6, Engineering sciences and reliability*. Oct 1986.
- [28] F. Porges. *HVAC engineer's handbook*, volume 11. Elsevier, 2001.